Comprehensive Optimization Model for Open Channel Design

Aly Khaled Aly Salem (Alykhaled@cu.edu.eg)
Cairo University Faculty of Engineering https://orcid.org/0000-0002-2295-9971
Yehya Emad Imam
Zewail City of Science and Technology
Ashraf Hassan Ghanem
Cairo University Faculty of Engineering
Abdallah Sadik Bazaraa
Cairo University Faculty of Engineering

Research Article

Keywords:

Posted Date: March 7th, 2022

DOI: https://doi.org/10.21203/rs.3.rs-1403688/v1

Version of Record: A version of this preprint was published at Water Resources Management on October 21st, 2022. See the published version at https://doi.org/10.1007/s11269-022-03323-w.

Comprehensive Optimization Model for Open Channel Design

Aly K. Salem · Yehya E. Imam · Ashraf H. Ghanem · Abdallah S. Bazaraa

Received: 28 February 2022 / Accepted: ...

Abstract Open channels are one of the most used water conveyance systems to deliver water for different purposes. Existing models for the design of open channels mainly assume uniform flow, focus on cross-section sizing, and generally decouple cross-section sizing from the selection of channel alignment and profile. This study developed an optimization model for a comprehensive design of conveyance channels. The model minimizes the sum of costs for earthwork, lining, water losses, and land acquisition; accounts for non-uniform, mixed-regime flow; and considers multiple geometric and hydraulic constraints. The model was validated using several idealized scenarios. The model potential in minimizing the cost of real open channel projects was demonstrated through application to an existing irrigation water transmission canal in Egypt (the Sheikh Zayed Canal). The results of validation scenarios matched the anticipated outcomes for channel profile and alignment and reproduced analytical solutions given in the literature for channel cross-section design. Application of the model to the Sheikh Zayed Canal gave a more optimal design; the OCCD model produced a design alternative with ~27% less cost than the constructed alternative.

Aly K. Salem: Irrigation and Hydraulics Department, Faculty of Engineering, Cairo University, Giza, Egypt.

Yehya E. Imam: Environmental Engineering Program, University of Science and Technology, Zewail City of Science and Technology, Giza, Egypt. Irrigation and Hydraulics Department, Faculty of Engineering, Cairo University, Giza, Egypt.

Ashraf H. Ghanem · Abdallah S. Bazaraa: Irrigation and Hydraulics Department, Faculty of Engineering, Cairo University, Giza, Egypt.

1. Introduction

Man-made open channels existed since at least the middle of the third millennium BC (Swamee and Chahar, 2013). They are still the most widely used water conveyance systems (Aksoy and Altan-Sakarya, 2006). Open channels may extend over a few kilometers to several hundreds of kilometers (e.g., Indira Gandhi Canal and Central Arizona Aqueduct). As open channel construction cost constitutes a major part of the cost of flood protection and water supply projects, optimization of open channel design is important for cost reduction and for achieving project economic feasibility, particularly for long-distance, large-capacity open channels. Furthermore, optimizing the design of open channels may aid in saving water lost by evaporation and seepage, which is particularly important for water supply projects in regions suffering from water scarcity (El Baradei and Al Sadeq, 2019).

The traditional design of open channels is a multi-stage process, which starts by selecting the channel alignment, then the channel profile, and finally the channel cross-section dimensions. For transmission channels with no intermediate water addition or abstraction, the selection of the channel alignment mainly aims to achieve the shortest path between the water source and destination locations provided that topography and obstructions along the shortest path are favorable. The selection of channel profile primarily depends on the topography; channel bed slopes are usually selected to match ground slope with mild slopes used in flat regions. Although flow in open channels is generally non-uniform, channel cross-section is typically designed based on flow resistance equations applied under uniform flow conditions (Swamee et al., 2000b; Akan, 2006; Chahar et al., 2007; Monadi et al., 2019).

Extensive research has been done on optimizing the channel cross-section, particularly for channels with rigid boundary (i.e., lined channels). In these channels, the primary design goal is typically to reduce the cross-section area and/or perimeter, as erosion control is not a major concern (Swamee et al., 2000a). By discarding freeboard, King et al. (1949); Chow (1959) derived the dimensions for the best hydraulic section (BHS) for different shapes, giving both minimum area and perimeter. Monadjemi (1994) proposed a more general approach for deriving the dimensions of the BHS using Lagrange's Method of Undetermined Multipliers. Froehlich (1994) accounted for depth and top-width constraints while determining the dimensions of the trapezoidal BHS. By considering freeboard, Guo and Hughes (1984) showed that the section with minimum total area differed from the section with the minimum total perimeter. Given this difference, subsequent studies aimed to optimize the cross-section by explicitly minimizing the total area and/or perimeter (i.e., lining and/or excavation costs) (Das, 2000; Swamee et al., 2000c; Jain et al., 2004; Bhattacharjya, 2005).

Trout (1982) ignored the excavation cost and focused on minimizing the lining cost with different unit prices for channel bed and sides. Das (2000) included the excavation cost with the lining cost and accounted for the difference in unit prices and roughness. Jain et al. (2004) considered both lining and excavation costs and added a maximum permissible velocity constraint. Bhattacharjya (2005) added the freeboard as a design variable to accommodate the depth fluctuation corresponding to a specified change in specific energy. Neglecting the differences in the lining material, Han et al. (2019) added the land acquisition cost to the lining and excavation costs and derived the general equation for the most economic section.

Discarding freeboard and based on the resistance equation formulated by Swamee (1994), Swamee et al. (2000c) considered a depth-dependent excavation cost with the lining cost, which made the optimal cross-section tend to be wider and shallower. Further improvement in cross-section optimization was attained by Swamee et al. (2000a) who combined the costs of water losses due to seepage and evaporation with lining and depth-dependent excavation costs.

Chahar (2006) accounted for the latter costs and proposed channel division into segments with different cross-sections to account for the decrease in discharge due to water losses along the channel. More recent studies examined the applicability of deterministic and heuristic optimization techniques in optimizing the channel cross-section. Adarsh and Sahana (2013) used the Probabilistic Global Search Lausanne algorithm, Tabari et al. (2014) and Tabari and Mari (2016) used the Direct Search algorithm, Niazkar and Afzali (2015) used the Honey Bee Mating Optimization algorithm, and El-Ghandour et al. (2020) used the Particle Swarm Optimization algorithm. Furthermore, Niazkar (2020) showed that artificial intelligence can be used to optimize the lined channels by comparing the results to explicit equations given by Swamee et al. (2000c), Aksoy and Altan-Sakarya (2006), and Niazkar and Afzali (2015).

Despite the considerable attention paid to the optimization of channel cross-section, few studies addressed the optimization of open channel alignment. Swamee and Chahar (2013) proposed the concept of balancing the cutting depth by equating the volume of excavation and embankment along individual segments of trapezoidal channels. Basu and Chahar (2013) applied the previous concept on channels with parabolic sections and introduced the concept of balancing the cutting depth along a certain length of the channel alignment. Swamee and Chahar (2015) reapplied the latter concept on the trapezoidal section to allow for feasible haulage length.

Most of the studies indicated earlier addressed the optimal channel cross-section as a separate problem from that of determining the optimal channel alignment and profile. Similarly, the few studies that examined optimal channel alignment decoupled it from the optimal cross-section design. Hence, these studies did not necessarily guarantee the optimal overall channel design. Furthermore, no automated optimization framework was developed in the studies that focused on alignment optimization; a manual trial approach was adopted.

The main objective of this study is to develop a model for the integrated design of transmission open channels. The model, referred to as the Open Channel Comprehensive Design (OCCD) model, accounts for the interdependence of the different channel parameters involved in the design process. To efficiently search the extensive design alternatives, the OCCD model applies an automated optimization technique instead of a traditional manual trial approach. Unlike previous studies, the OCCD model accounts for a non-uniform, mixed-flow regime resulting from changes in the channel profile and/or cross-section.

The developed model combines several sub-modules with a genetic algorithm module to minimize selected or combined cost components including the cost of earthwork, lining, land acquisition, and water losses. The OCCD model includes several geometric and hydraulic constraints; e.g., restricted zones, maximum depth, maximum velocity, and limits on changes in cross-section dimensions. The results of the OCCD model were validated using several idealized scenarios. Furthermore, the OCCD model performance was assessed by applying the OCCD model to an irrigation water transmission channel in Egypt, the Sheikh Zayed Canal (SZC).

This paper is structured as follows. The next section presents the model components and modules. The following section describes the model validation scenarios and performance. Afterwards, the SZC case study is described, and the results of several modelling scenarios are compared to the existing canal design. Finally, conclusions and recommendations for future work are given.

2. Methods

2.1 Modeling Framework

The OCCD model consists of three main modules which include the Optimization Controller (OC) module, the Hydraulic Simulation (HS) module, and the Quantity and Cost (QC) module (Fig. 1). The OC module generates an initial set of channel design alternatives. For each alternative, the HS module simulates the flow depth and velocity along the entire channel. The QC module then estimates the needed freeboard, bank level, excavation, fill and lining quantities, land acquisition extent, and water losses. The total cost for each alternative is subsequently calculated by the QC module and relayed back to the OC module. With the total cost of all design alternatives, optimization operators are applied to the population to produce the next generation with more optimal design alternatives. The model proceeds with repeating this cycle until stopping criteria are satisfied and the optimal design alternative is identified.

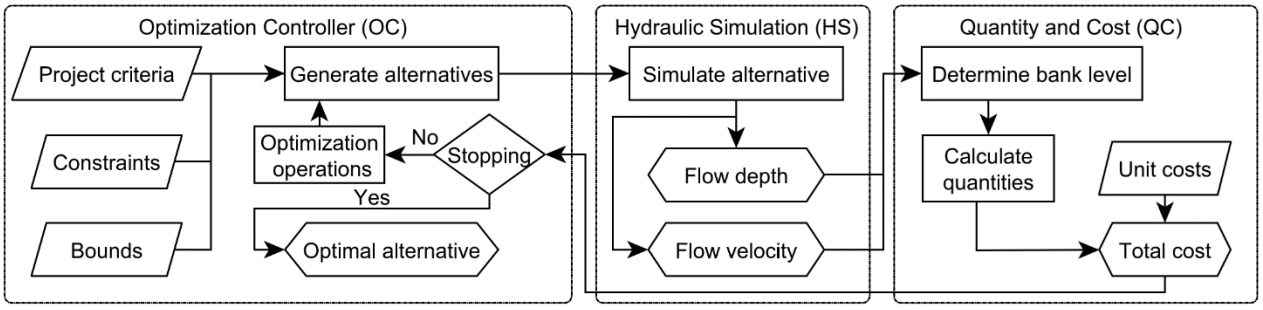

Fig. 1: Workflow of the OCCD model.

2.2 Design Variables

The OCCD model divides the channel to be designed into multiple straight reaches with trapezoidal cross-sections. Bed width, side slope, and longitudinal slope are kept constant along each reach but can vary between reaches. Transitions in cross-section dimensions, slope, horizontal alignment (i.e., reach direction) and bed level occur at the intermediate junctions connecting the reaches. The length of the transitions between reaches is neglected compared to reach lengths. However, the energy loss and the change in water surface elevation at the transitions are accounted for in the OCCD model.

For each reach $i = 1,2,\ldots,n_r$, the design variables are the reach bed width (b_i), side slope (t_i), and upstream bed elevation (Z_i). For each intermediate junction $j = 1,2,\ldots,n_r - 1$, the design variables are the coordinates (x_j, y_j) and the bed drop or rise d_j (where $d_j > 0$ represents a drop). The last design variable is the downstream bed elevation of the last reach (Z_e); i.e., bed elevation at the destination point. For the reaches other than the last reach, the downstream bed elevation of the i^{th} reach is calculated by adding the bed drop/rise at the intermediate junction $d_{j=i}$ to the upstream bed elevation of the subsequent reach Z_{i+1}. The full set of design variables and their count is summarized in Tab. 1.

Table 1: Full set of design variables and their count as a function of the number of reaches n_r.

Variable	Symbol	Variable Count
Intermediate junction coordinates	x_j, y_j	$2 \times n_r - 2$
Reach bed width	b_i	n_r
Reach side slope	t_i	n_r
Reach upstream bed elevation	Z_i	n_r
Bed elevation at the destination point	Z_e	1
Intermediate junction drop/rise	d_j	$n_r - 1$

Increasing the number of reaches gives the OCCD model the flexibility to form more complex channel alignment (Fig. 2). Also, using more reaches allows the model to select the channel profile and cross-sections that better adapt to the topography. However, using more reaches increases the complexity of the optimization process; the total number of design variables n_v increases linearly with the number of reaches according to Eq. 1,

$$n_V = 6n_r - 2 \tag{1}$$

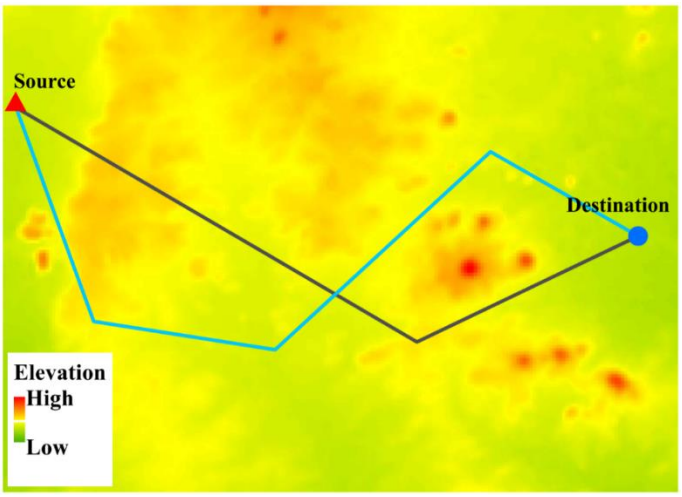

Fig. 2: Illustration of the possibility of forming more complex channel alignments by using a higher number of reaches. The black line shows a channel alignment with two reaches ($n_r = 2$). The blue line shows a more sinuous channel with four reaches ($n_r = 4$). The red marker indicates the starting point of the channel (i.e., the source). The blue marker indicates the channel end point (i.e., the destination). Color shading represents ground elevation.

2.3 Optimization Controller Module

2.3.1 Objective Function and Constraints

The OCCD model applies an optimization scheme to minimize the overall cost of the open channel that is being designed. The objective function of the optimization scheme can be represented mathematically as:

$$\text{Minimize} \qquad C_{tot} = f_1 C_E + f_2 C_L + f_3 C_W + f_4 C_A \tag{2}$$

where C_{tot} is the total channel cost, C_E is the earthwork cost including excavation cost C_x and fill cost C_f, C_L is the lining cost, C_W is the cost incurred by water loss from the channel, and C_A is the land acquisition cost. In Eq. 2, f_k with $k = 1$ to 4 is a binary factor that can be set to 0 to exclude specific cost items.

To determine the optimal values of the design variables, the OCCD model applies the objective function given by Eq. 2, subject to a number of geometric and hydraulic constraints that ensure the feasibility of the results. Hydraulic constraints prevent near-critical flow regime and limit the water depth and velocity to user-specified thresholds. Geometric constraints prevent undesired channel geometries that may be generated during the application of the optimization scheme; e.g., self-intersecting alignments, passage through restricted zones, and adverse slopes. Geometric constraints also enforce an upper limit on the ratio of bed widths for successive reaches to avoid excessive expansions and contractions in cross-sections.

The OCCD model implements the above constraints through different schemes. To produce feasible design alternatives with non-adverse slopes and reasonable changes in bed width between reaches, the OCCD model applies the linear inequalities,

$$Z_i - (Z_{i+1} + d_i) \geq 0 \tag{3}$$

$$Z_{n_r} - Z_e \geq 0 \tag{4}$$

$$\gamma_e \geq \frac{b_{i+1}}{b_i} \geq \gamma_c \tag{5}$$

where $\gamma_e \geq 1$ is the maximum expansion ratio and $\gamma_c \leq 1$ is the minimum contraction ratio for bed width. For maximum water depth and velocity constraints, the OCCD model applies a penalty to the design alternatives that violate these constraints. Finally, the OCCD model eliminates the design alternatives that violate constraints related to near-critical slope, self-intersection, and restricted zones.

Besides the above constraints, the OCCD model enforces lower and upper bounds for all design variables. Furthermore, for efficiency, the optimization scheme uses an integer instead of real-valued variables. A unit step maps to a discrete change of 10 m for junction coordinates, 0.25 m for bed width, 0.1 for side slope, and 0.1 m for bed drop/rise at junctions.

2.3.2 Optimization Scheme

The genetic algorithm (GA) was selected as the optimization scheme for the OCCD model due to its ability to solve complicated non-linear problems, and its extensive use in engineering applications (Simpson et al., 1994; Yeo and Agyei, 1998; Jain et al., 2004; Yeniay, 2005). As an evolutionary algorithm, the main advantage of the GA is that it does not require objective function derivatives and can handle the optimization of non-smooth objective functions (Haupt and Haupt, 2003; Kramer, 2017).

The OCCD model utilizes the Matlab GA toolbox (Mathworks, 2014). The GA implementation in the OCCD model starts by semi-randomly generating multiple sets of design variables (i.e., a population of design alternatives) satisfying specified bounds and constraints. The GA subsequently calls the Hydraulic Simulation (HS) and Quantity and Cost (QC) modules to calculate the fitness value of each individual design alternative then sends this value back to the GA to produce a new generation. The GA applies selection, crossover, and mutation operators to produce the next generation of design alternatives. The selection operator draws the most fit individuals (i.e, parents) from the current population and directly passes a limited number representing the most elite individuals to the next generation. The remaining parents are paired and combined by the crossover operator to generate new individuals. To increase the diversity and avoid quickly getting trapped in local minima, the mutation operator then randomly alters some of the parents' genes. The process is repeated and new generations are produced until the average relative change in the fitness values remains below a set threshold for a specified number of generations (known as stalled generations).

As indicated earlier, the GA semi-randomly generates the initial population. While reach bed width and side slope are randomly generated (subject to the previously mentioned bounds and constraints), a deterministic scheme is used to define coordinates and elevations of junctions between reaches for the design alternatives of the initial population. This scheme uniformly locates junction coordinates along paths given by polynomial functions that cover a large swath surrounding the channel end points (see example in Fig. 3). Bed elevations at junctions are then determined based on the average slope between the channel end points. This deterministic definition of junctions avoids the generation of infeasible self-intersecting alignments and ensures that the entire search domain is properly sampled. For subsequent generations, self-intersecting alignments may be formed by the GA cross-over and mutation operators. A sub-module of the OCCD model identifies the self-intersections and eliminate the corresponding alternatives. Similarly, alternatives passing through restricted zones as well as alternatives with near-critical slopes are identified and eliminated before the application of the Hydraulic Simulation module which is described next.

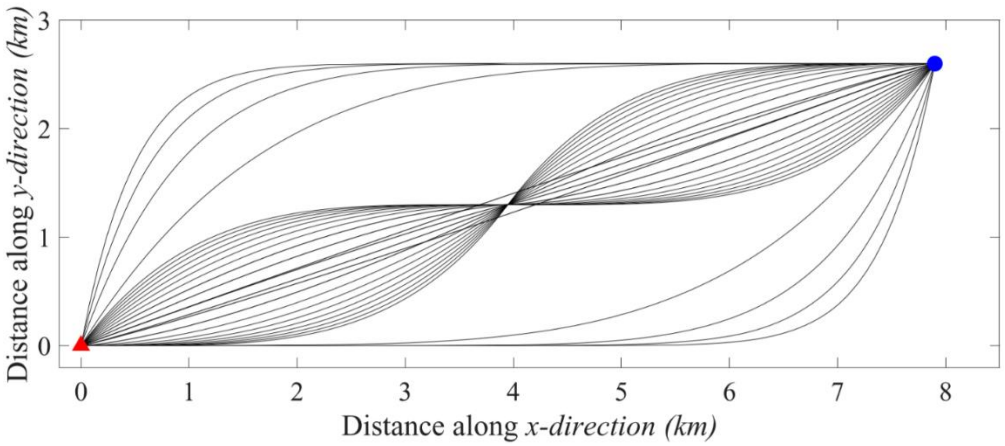

Fig. 3: Plan view of paths used to define reach junctions for the design alternatives of the initial population. The red marker indicates the starting point of the channel. The blue marker indicates the channel end point.

2.4 Hydraulic Simulation Module

For each feasible design alternative, the Hydraulic Simulation (HS) module determines the water surface elevation along the channel based on steady, one-dimensional, gradually varied flow analysis given by Eq. 6 (King et al., 1949),

$$\frac{dy}{dx} = \frac{S_o - S_f}{1 - F_r^2} \tag{6}$$

where $\frac{dy}{dx}$ is the rate of change of water depth with distance x along the channel reach, S_o is the reach bed slope, S_f is the friction slope, and F_r is the Froude number.

The OCCD model applies a finite difference scheme to solve Eq. 6. Discretization of each reach of length L is based on a geometric series scheme that produces variable computational intervals Δl ranging between specified minimum (Δl_{min}) and maximum (Δl_{max}) values (Fig. 4). This discretization scheme provides better accuracy for possible near-critical flow at the start and/or end of the channel reaches without significant increases in the computational time needed for applying small uniform intervals along the entire reach.

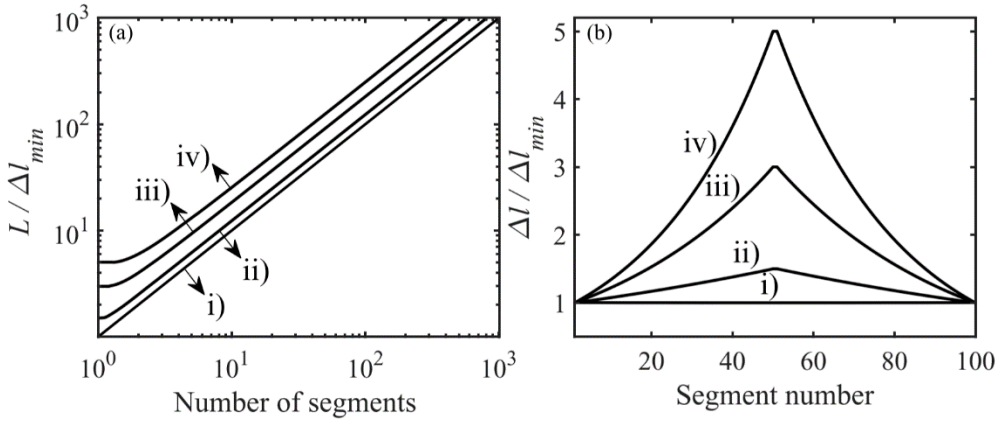

Fig. 4: (a) Relative reach length $L/\Delta l_{min}$ attained by using i) $\Delta l_{max}/\Delta l_{min} = 1$, ii) $\Delta l_{max}/\Delta l_{min} = 1.5$, iii) $\Delta l_{max}/\Delta l_{min} = 3$, and iv) $\Delta l_{max}/\Delta l_{min} = 5$, and (b) Corresponding computational intervals along a reach with 100 segments.

The HS module performs mixed flow regime analysis. Sub-critical flow simulation starts with the normal depth imposed as a boundary condition at the downstream end of the channel. The solution proceeds in the upstream direction. Energy conservation is applied at transitions between reaches to estimate the flow depth at the downstream ends of upstream reaches. Energy losses due to expansion/contraction at reach transitions are estimated using (HEC, 2016),

$$H_l = K_l \left| \frac{V_1^2}{2g} - \frac{V_2^2}{2g} \right| \tag{7}$$

where V_1 and V_2 are the flow velocities upstream and downstream of the transition, respectively, and K_l is the head loss coefficient which is set to 0.1 for contraction $(V_2 > V_1)$ and 0.3 for expansion $(V_2 < V_1)$.

During the sub-critical flow simulation, computational nodes with near-critical depth are flagged for further analysis. After the sub-critical simulation concludes, a super-critical flow simulation starts from the first upstream node that was flagged during the sub-critical simulation and continues in the downstream direction. The super-critical simulation is interrupted when a valid sub-critical flow depth with higher specific force is found, and a hydraulic jump (with a negligible length) is assumed to occur between the super-critical and sub-critical depths. The super-critical flow simulation resumes at the next flagged nodes if any.

The HS module was implemented in Matlab for efficient integration with the Optimization Controller module. Hydraulic simulation results were validated for different flow conditions through comparison to results from HEC-RAS simulations (an example is illustrated in Fig. 5).

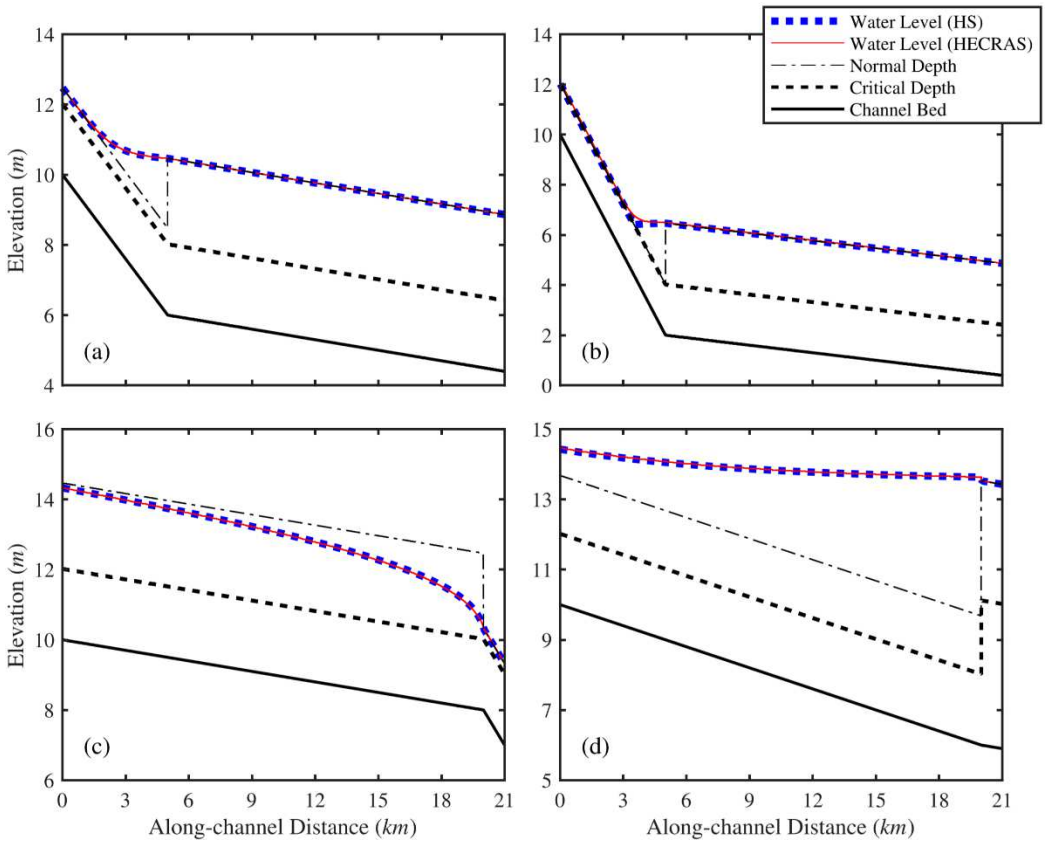

Fig. 5: Comparison of along-channel water surface elevation simulated with the OCCD HS module and HEC-RAS for a channel with a) a mild-sloped reach connected to a reach with milder slope, b) a steep reach connected to a mild-sloped reach, c) a mild-sloped reach ending with a critical slope and d) a mild-sloped reach ending with a contraction and milder slope.

2.5 Quantity and Cost Module

Based on the hydraulic simulation results along with the alignment, profile, and cross-section for each reach, the Quantity and Cost (QC) module computes the water surface elevation with respect to the ground level (Fig. 6). For a specified freeboard (F_b), the QC module then calculates the earthwork (i.e., excavation and fill), lining, and land acquisition quantities. Each of these quantities is calculated at uniformly-spaced sampling nodes after interpolating the HS module results obtained at the computational nodes. The quantities are then summed over the reaches and multiplied by the unit price of each cost item to give total costs as follows

$$C_x = U_X\left(\sum_{i=1}^{n_r}\sum_{k=1}^{m_i}\frac{A_{x_{k,i}} + A_{x_{k+1,i}}}{2}\Delta x\right) + U_D\left(\sum_{i=1}^{n_r}\sum_{k=1}^{m_i}\frac{A_{x_{k,i}} \times \bar{Y_{k,i}} + A_{x_{k+1,i}} \times \bar{Y_{k+1,i}}}{2}\Delta x\right) \quad (8)$$

$$C_f = U_F\left(\sum_{i=1}^{n_r}\sum_{k=1}^{m_i}\frac{A_{f_{k,i}} + A_{f_{k+1,i}}}{2}\Delta x\right) \quad (9)\ \&$$

$$C_L = U_L\left(\sum_{i=1}^{n_r}\sum_{k=1}^{m_i}\frac{\ell_{k,i} + \ell_{k+1,i}}{2}\Delta x\right) \quad (10)$$

$$C_A = \left(\sum_{i=1}^{n_r}\sum_{k=1}^{m_i}\frac{T_{k,i} \times U_{A_{k,i}} + T_{k+1,i} \times U_{A_{k+1,i}}}{2}\Delta x\right) \quad (11)$$

$$C_W = U_W \times N\left[\sum_{i=1}^{n_r}\sum_{k=1}^{m_i}\left(\frac{q_{s_{k,i}} + q_{s_{k+1,i}}}{2} + \frac{q_{v_{k,i}} + q_{v_{k+1,i}}}{2}\right)\Delta x\right] \quad (12)$$

where Δx is the interval between the sampling nodes, $i = 1,2 \ldots n_r$ is the reach index, $k = 1,2, \ldots m_i$ is the sampling node index; U_X is the unit cost of excavation at ground level; U_D is the excavation cost increment per unit depth; U_F, U_L, U_A, and U_W are the unit costs for fill, lining, land acquisition, and water losses, respectively; A_x and A_f are the excavation and fill areas, respectively; ℓ is lining length within channel cross-section; q_s and q_v are the amounts of water lost due to seepage and evaporation per unit length of the channel, respectively; $\bar{Y}$ is the depth from the ground surface to the centroid of the excavated area; T is the total channel width including banks; and N is the useful lifetime of the channel.

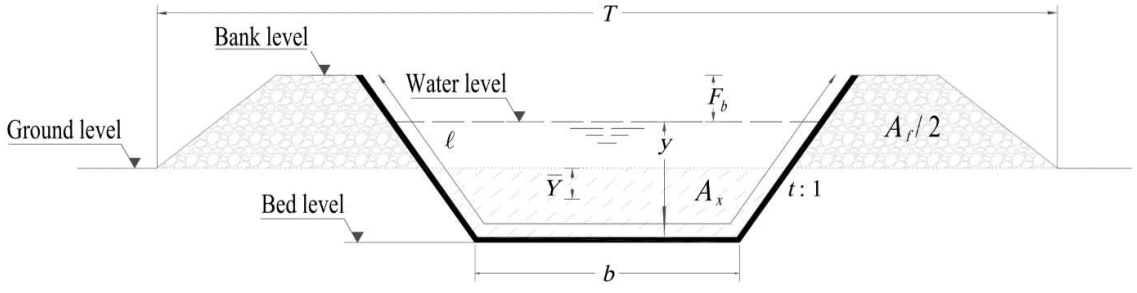

Fig. 6: Schematic view of a typical channel section. Indicated on the schematic are the dimensions used in the Quantity and Cost (QC) module.

3. Model Validation

3.1 Validation Scenarios

Seven validation scenarios VS 1 to VS 7 were conducted to confirm the ability of the OCCD model to identify optimal channel design parameters (Tab. 2). In scenario VS 1, the objective was to optimize the cross-section to achieve the minimum lining cost subject to a maximum water depth constraint as presented by Froehlich (1994). In the second validation scenario VS 2, the objective was to optimize the cross-section considering lining and depth-dependent excavation costs. Results were compared to the regression equations obtained by Niazkar and Afzali (2015) using the Honey Bee Mating Optimization algorithm. For the next scenario VS 3, the cross-section was optimized to minimize lining, excavation, and land acquisition costs considering freeboard. The results were compared to the analytical solution derived by Han et al. (2019) for different values of side slope.

Validation scenario VS 4 aimed to identify the channel alignment and profile that minimize the excavation cost and to examine the effect of changing the number of reaches nr on model results. In scenario VS 5, the objective was to determine the channel alignment that minimizes lining and land acquisition costs. To achieve this objective, scenario VS 5 used a region with a binary low/high land cost (Fig. 7a). Two cases were considered with different high-to-low land cost ratios.

Similar to VS 5, scenario VS 6 had the same objective but with the addition of restricted zones (Fig. 7b). Scenario VS 6 also examined the effect of the number of reaches n_r on the identified optimal channel alignment. Finally, the objective of scenario VS 7 was to optimize all the design parameters to achieve the minimum lining and earthwork costs subject to a maximum velocity constraint V_{max} (Tab. 2).

The topography in scenarios VS 2 and VS 3 consisted of a straight valley-like terrain with a uniform longitudinal slope of 10 cm/km with valley sides rising to the edge of the search domain with a slope of 5 m/km (Fig. 8a). Topography in scenario VS 4 consisted of a winding valley-like terrain with variable longitudinal slopes ranging from 1 cm/km to 9 cm/km (Fig. 8b). The topography in VS 7 was a relatively steep terrain with a uniform, the uni-directional slope of 1.3 m/km (Fig. 8c). The topography does not influence the results of scenarios VS 1, VS 5, and VS 6 as the earthwork cost was excluded from these scenarios.

Validation scenarios VS 4 to VS 7 were conducted using a Manning roughness coefficient $n = 0.013$ and a volumetric flow rate $Q = 80$ m3/s. The OCCD model results for scenarios VS 1, VS 2, and VS 3 were summarized using the parameters λ, α, β, U_L^*, and U_D^*. The parameter $\lambda = \left(nQ/\sqrt{S_o}\right)^{3/8}$ is a length scale that represents the size of the required cross-section where S_o is the longitudinal slope. The dimensionless parameters $\beta = b/y$ and $\alpha = F/y$ represent the bed width to depth ratio and the freeboard to depth ratio, respectively. Finally, the parameters $U_L^* = U_L/U_X\lambda$ and $U_D^* = U_D\lambda/U_X$ represent the normalized cost of lining and normalized cost of excavation with depth, respectively. The ratio U_L^*/U_D^* gives the relative costs of depth-dependent excavation and lining. Higher values of U_L^*/U_D^* indicate greater importance for the increase of excavation cost with depth relative to the lining cost.

Scenario	VS 1	VS 2	VS 3	VS 4	VS 5	VS 6	VS 7
Target cost	Not relevant	Straight valley (Fig. 8a)		Winding valley (Fig. 8b)	Not relevant		Uniformly-sloped (Fig. 8c)
Minimizing costs	Lining	Lining and depth-dependent excavation	Lining, excavation, and land	Excavation	Lining and land cost		Lining and earthwork
Design variables	Cross-section		Bed width	Alignment and profile	Alignment		Alignment, profile, and cross-section
Fixed Parameters	Alignment and profile		Alignment, profile and side slope	Cross-section	Profile and cross-section		-
Unit cost	-	$U_L = 2$ $U_X = 1$ $U_D = variable$	$U_L = 2$ $U_X = 1$ $U_A = 0.5$	-	$U_L = 10$ $U_A^{low} = 0.1$	$U_L = 10$ $U_A^{low} = 0.1$ $U_A^{high} = 10$	$U_L = 10$ $U_X = 1$ $U_D = 0.12$ $U_F = 1.4$
Anticipated outcomes	Match results of Froehlich (1994)	Match empirical equations by Niazkar and Afzali (2015)	Match results of Han et al. (2019)	Alignment follows the valley and profile follows the ground	Give shortest alignment within the area of low cost land	Give shortest alignment within the area of low-cost land that does not cross restricted zones	By imposing smaller V_{max}, the model selects milder slopes, widens the cross-section, and may create bed drops

Table 2: Parameters for validation scenario and anticipated outcomes.

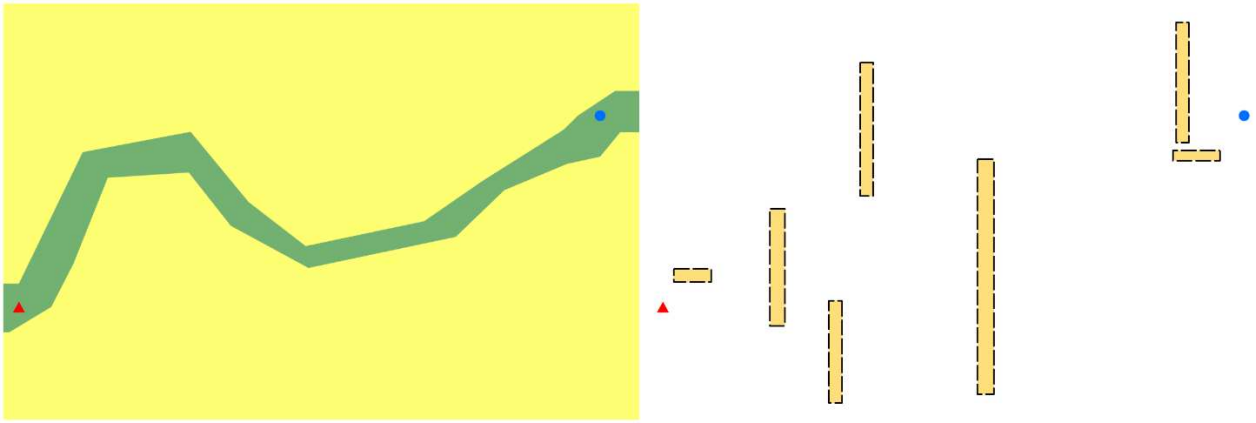

(a) (b)

Fig. 7: a) Spatial distribution of land cost used in validation scenario VS 5. Green shading denotes a land of low cost. Yellow shading denotes a land of higher cost. b) Location of restricted zones (orange patches) used in validation scenario VS 6.

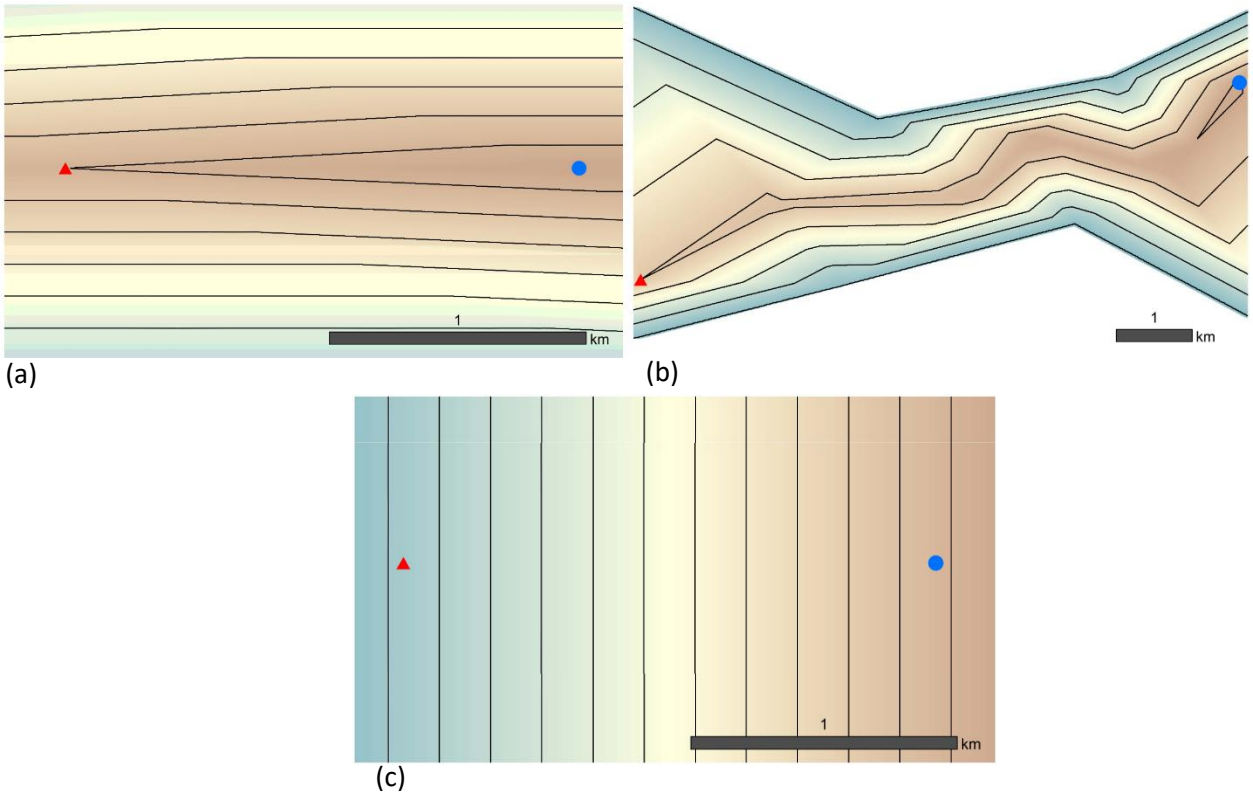

(a) (b)

(c)

Fig. 8: Topography for validation scenarios a) VS 2, b) VS 3, and c) VS 6. Green shading indicates higher ground. Brown shading indicates lower ground. Solid lines represent elevation contours with 0.25 m intervals. The red triangle denotes the source and the blue dot denotes the destination.

To compare the OCCD model results for VS 1 to VS 3 to the literature, the widely used Nash–Sutcliffe efficiency coefficient (NSE) was used (McCuen et al., 2006). The NSE was calculated using,

$$NSE = 1 - \frac{\sum_{i=1}^{n}\left(y_{a_i} - y_{m_i}\right)^2}{\sum_{i=1}^{n}\left(y_{a_i} - \bar{y_{a_i}}\right)^2} \quad (13)$$

where y_{m_i} represents the OCCD model results, y_{a_i} represents the analytical solution from the literature, and $\bar{y_{a_i}}$ is the mean of the y_{a_i} values. The NSE ranges from -∞ to 1, where 1 indicates a perfect match between the OCCD model results and the analytical solution given in the literature.

3.2 Model Performance

Results of scenario VS 1 show that, for a given cross-section scale λ, the bed width b giving minimal lining cost decreased with the increase of the maximum imposed depth y_{max} up to $y_{max} = 0.968\,\lambda$ (Fig. 9a). For higher values of y_{max}, the optimal bed width remained constant and the depth corresponded to y_{max}. The side slope t oscillated around $1/\sqrt{3}$ for small values of y_{max}/λ with the magnitude of the oscillations becoming smaller with the increase in y_{max}/λ. For $y_{max}/\lambda \gtrsim 0.8$, the side slope attained a constant value of $t = 1/\sqrt{3}$ (Fig. 9b). The model results for the VS 1 scenario matched the analytical solution by Froehlich (1994) with a high NSE of 0.999 for bed width (Fig. 9).

For scenario VS 2, the OCCD model shows that, with a higher relative cost for depth-dependent excavation (U_D^*/U_L^*), a cross-section of scale λ required larger bed width to depth ratio β (i.e. shallower depth, larger bed width), and steeper side slope to have minimal lining and excavation costs (Fig. 10a-c). These trends are the same as those revealed by the regression equations given by Niazkar and Afzali (2015) over the equations' range of applicability $0 < U_D^*/U_L^* < 2$. However, compared to the regression equations, the OCCD model results show less dependence on U_D^*/U_L^* when its value approaches 2 (Fig. 10a-b). For flow depth, the results of the OCCD model are more accurate than the regression equations; the latter gives depths that deviate from the values obtained with the Manning equation using the bed widths and side slopes from the regression equations (Fig. 10c). This deviation leads to inaccurate total cost estimation. Correction of the depth and the total cost from the equations by Niazkar and Afzali (2015) shows that the OCCD model produces more optimal solutions with up to 1.1% lower cost.

The results of VS 3 show that for any value of side slope, β increased with the increase of λ for $\alpha = 0$, and decreased when $\alpha \geq 0.1$ (Fig. 11). Also, the results show that the rate of change of β with respect to λ decreased (i.e., became less sensitive) with the increase of the side slope (t) (Fig. 11). The VS 3 results matched the analytical equations produced by Han et al. (2019), with an average NSE of 0.95, 0.85 and 0.52 for $t = 0.5$, $t = 1$ and $t = 1.5$, respectively.

In VS 4.1, the OCCD model generated a non-straight alignment to minimize the excavation through the terrain (Fig. 12a), and to reduce the cost by 78% compared to the straight alignment. Increasing the number of reaches (n_r) to 8 in VS 4.2 gave the OCCD model more flexibility to produce an alignment that closely followed the path of the winding valley (Fig. 12a), and reduced the cost by 14% than VS 4.1. For VS 4.2, the profile coincided with the ground (Fig. 12c) with less excavation than VS 4.1 (Fig. 12b). These results confirmed the OCCD model ability to determine the optimum alignment and profile that minimize the excavation cost.

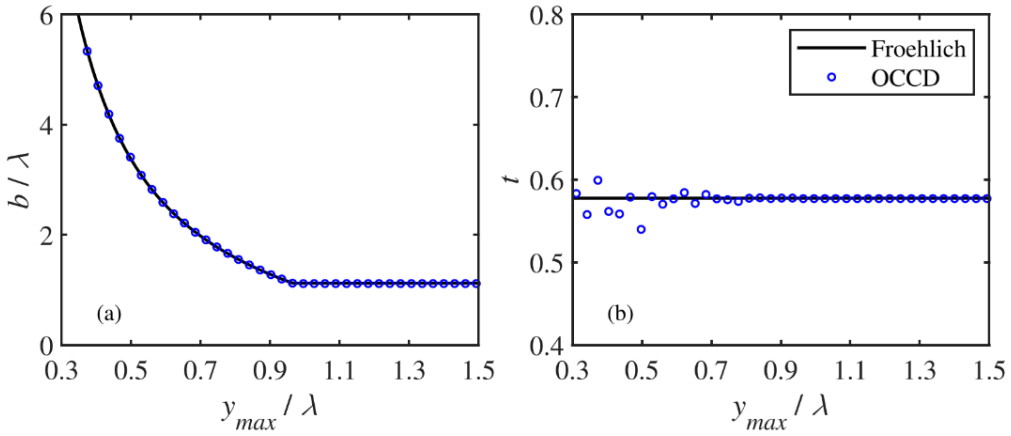

Fig. 9: OCCD model results for scenario VS 1 versus analytical solution by Froehlich (1994). Shown are the a) bed width and b) side slope for minimum lining cost.

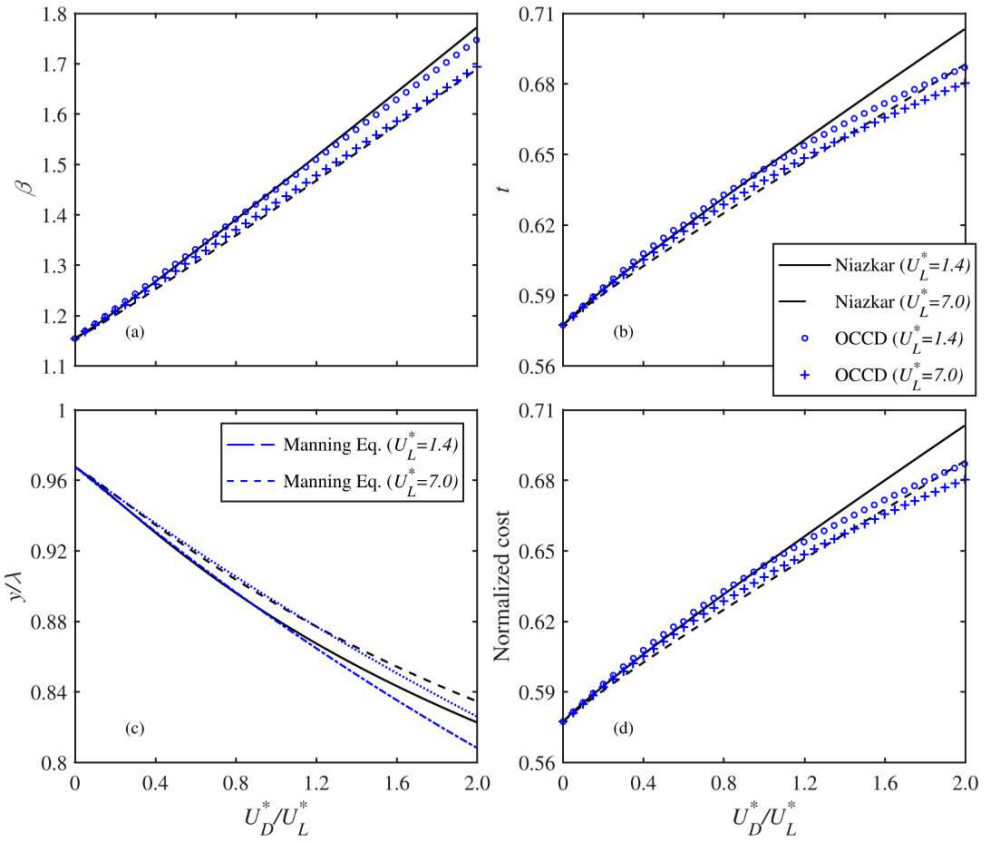

Fig. 10: OCCD model results (markers) for scenario VS 2 versus values from regression equations by Niazkar and Afzali (2015) (solid lines). Shown are the a) bed width to depth ratio β, b) side slope, and c) depth for minimum lining and depth-dependent excavation costs. Also shown in panel d) is the total cost normalized by the cost when excavation cost is independent of depth (i.e., $U_D = 0$).

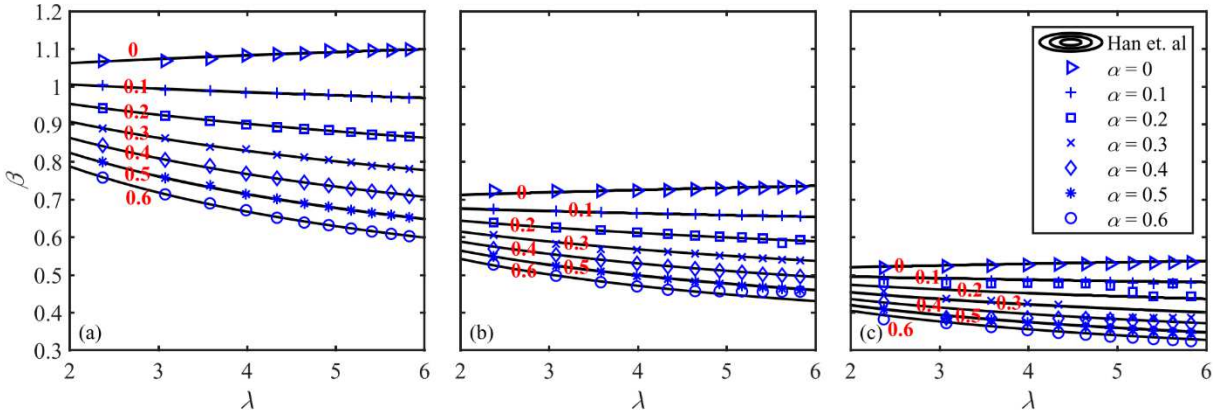

Fig. 11: OCCD model results (markers) for scenario VS 3 versus analytical solution by Han et al. (2019) (solid lines). Shown is the variation of the optimal bed width to depth ratio β with the cross-section scale λ for the side slopes a) $t = 0.5$, b) $t = 1$, and c) $t = 1.5$. Solid lines represent different freeboard-to-depth ratios α. Values of β correspond to the minimum lining, excavation, and land acquisition costs for the unit $U_L/U_X = 2$ m and $U_A/U_X = 0.5$ m.

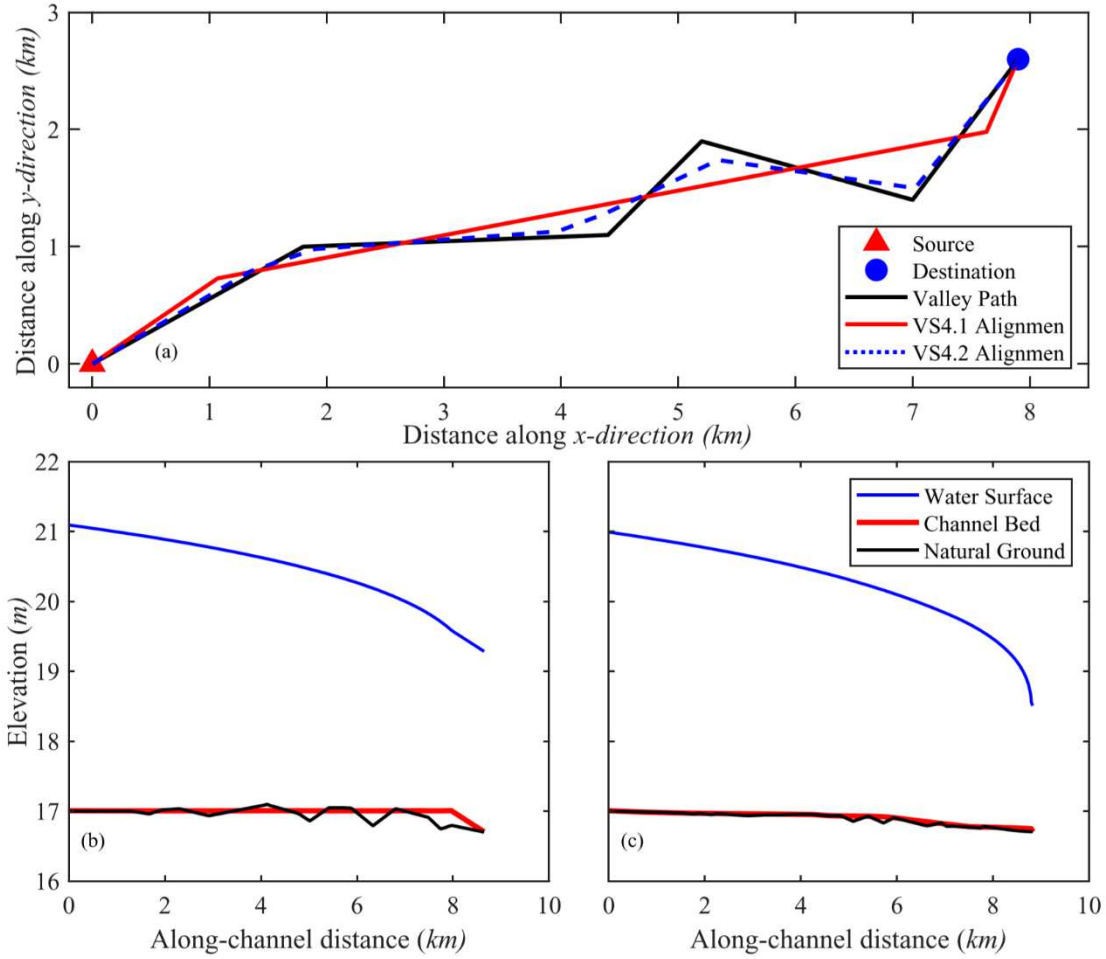

Fig. 12: a) VS 4 alignment, b) VS 4.1 profile and c) VS 4.2 profile.

In VS 5, the OCCD model successfully handled the spatial variation of the land acquisition cost. For VS 5.1 with a high-to-low (HL) land cost ratio of 3.0, the lining cost dominated over land acquisition cost leading to alignment that partly crossed through the high cost land (Fig. 13a). This alignment produced a total cost 38% lower than the straight alignment. By increasing the HL land cost ratio from 3 to 100 in VS 5.2, the land acquisition cost became much more significant than the lining cost. The corresponding alignment followed a longer path completely within the low cost land (Fig. 13a). This alignment produced a total cost 94% lower than the straight alignment.

In VS 6, the OCCD model properly identified the location of restricted zones and selected the shortest alignment within the low cost land without crossing the restricted zones (Fig. 13b). Also, by increasing n_r from 6 in VS 6.1 to 15 in VS 6.2, the OCCD model was able to form a more complex alignment with a reduced cost of 40%.

In VS 7, the optimum alignment produced by the OCCD model was the shortest path connecting the source and the destination for all three sub-scenarios (Fig. 14a). However, the optimum profile and cross-section varied based on the maximum velocity (V_{max}). With no velocity constraint in VS 7.1, the OCCD model minimized the cost by producing a profile with successively increasing bed slope (Fig. 14b). This allowed the flow to accelerate, velocity to increase, and cross-section area to decrease. The velocity at the downstream reached 4.5 m/s, which can damage the filler in joints between the lining panels. By limiting the maximum velocity in VS 7.2 to 3 m/s, the OCCD model produced an almost constant bed slope, which induced an approximately uniform flow (Fig. 14c). Also, a wider cross-section was produced to accommodate the flow, with a total cost ~20 % higher than VS 7.1.

Table 3: Results for scenarios VS 7.1 to VS 7.3. Cost difference is relative to cost in scenario VS 7.1.

Sub-scenario	V_{max}	Long. slope	Bed width	Side slope	Drop	Cost Difference
	(m/s)	(cm/km)	(m)	$(H:V)$	(m)	(%)
VS 7.1	∞	$0 \sim 182.7$	3.8	0.56: 1	0	0
VS 7.2	3	62.0	4.9	0.59: 1	0	20.4
VS 7.3	2	21.1	6.4	0.51: 1	0.2	56.1

Lowering the velocity to 2 m/s in VS 7.3, the OCCD model produced a profile with a bed drop of 0.2 m (Fig. 14d). A wider cross-section was produced and the cost increased by 56 % beyond the cost in VS 7.1. summaries the results of all three sub-scenarios, listing the allowable velocities, the optimum profile and cross-section dimensions, and the percentages of cost increment relative to VS 7.1.

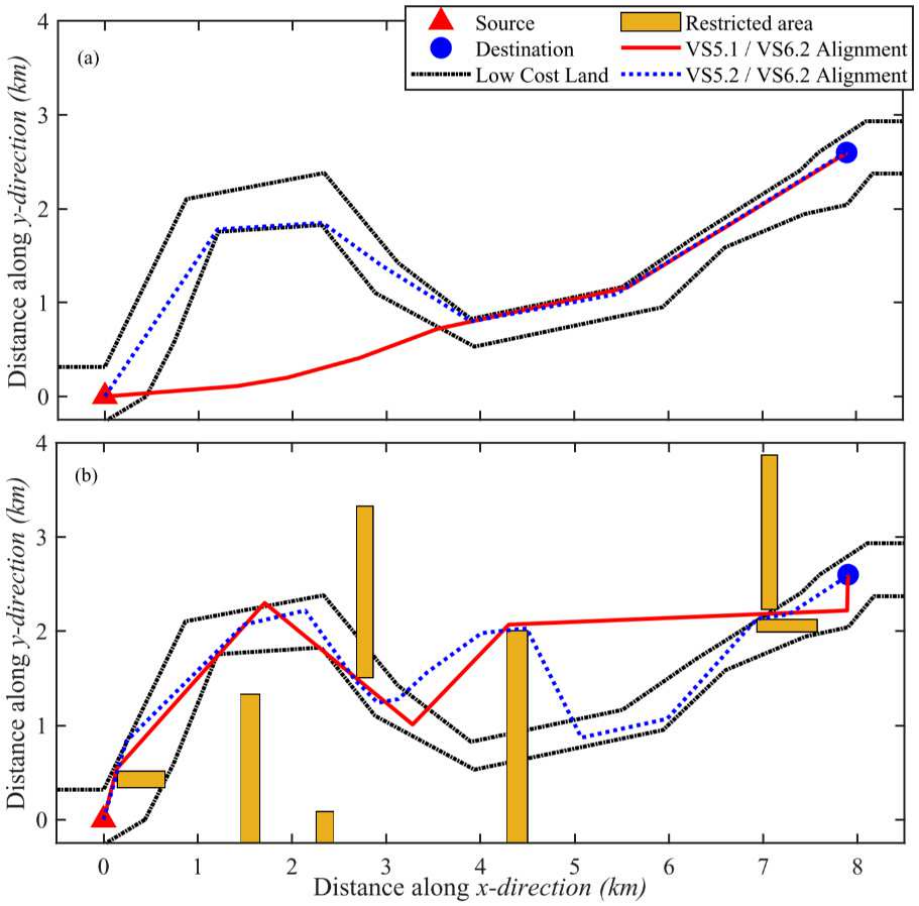

Fig. 13: Results of a) VS 5 and b) VS 6.

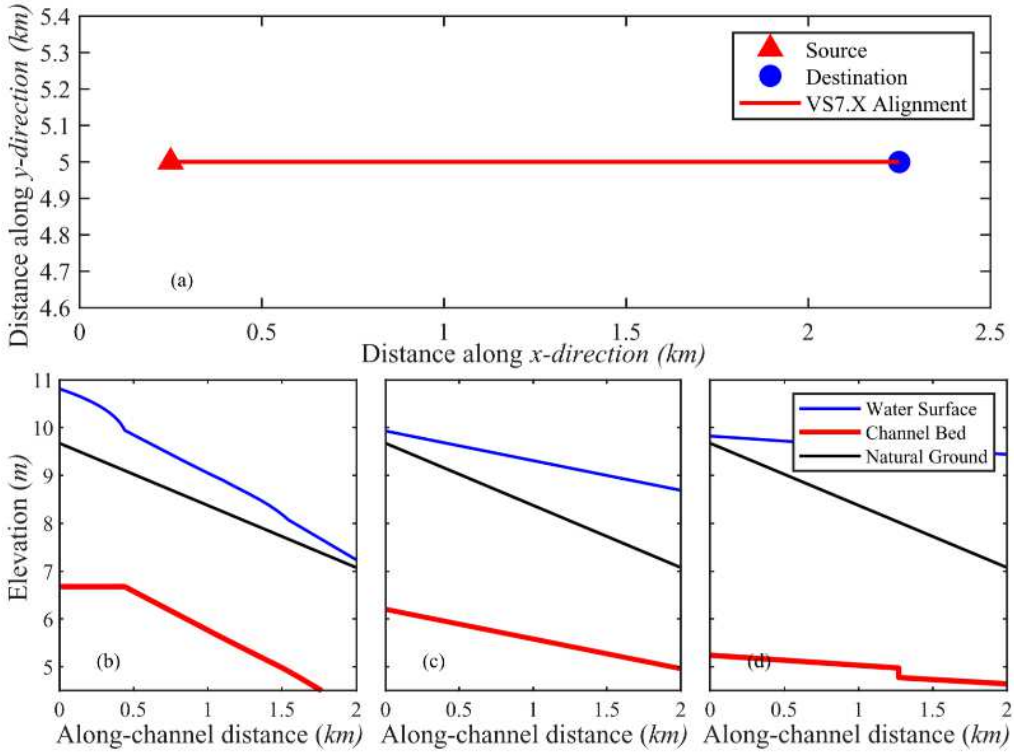

Fig. 14: Results of a) VS 7 alignment, b) VS 7.1 profile, c) VS 7.2 profile and d) VS 7.3 profile.

4. Model Application

To demonstrate the OCCD model potential in minimizing the total cost of real projects, the model was applied to an irrigation water conveyance channel in Egypt, the Sheikh Zayed Canal (SZC). This section gives a description of SZC and presents the implementation of the OCCD model to SZC. Model results are also analyzed and compared to the existing SZC design.

4.1 Canal Characteristics

SZC delivers irrigation water to 540,000 feddan in the western desert of Egypt and is the main component of the Toshka Agricultural Development Project which started in 1998 (Wahby, 2002). The SZC is located $250\,km$ south of Aswan and is supplied by water from Lake Nasser via the Mubarak Pumping Station (Fig. 15). The SZC extends for about 50 km and runs mostly parallel to Toshka Bay at a distance ranging from about 2.4 to $5.5\,km$ from the Bay boundary (Fig. 15). The first segment of the canal is a transitional vertical-walled canal with a length of approximately $2.7\,km$. The rest of SZC is the main stem and is the focus of this paper. SZC consists of 23 reaches connected by curves with radii ranging between 400 and $1600\,m$. The main stem has a trapezoidal cross-section with a bed width of $30\,m$, a side slope $t = 2$, and a bed slope of $10\,cm/km$ (Wahby, 2002). The canal has a design capacity of $334\,m^3/sec$ with a maximum water depth of $6\,m$ and a freeboard of $1\,m$ (El Baradei and Al Sadeq, 2019). To reduce seepage losses, the SZC was lined with a $0.2\,m$ concrete layer placed on top of $1\,mm$ thick polyethylene sheets which were in turn laid on top of a $0.2\,m$ thick compacted and stabilized soil.

Pre-construction satellite imagery for the SZC domain revealed no distinct land use in the region except for some scattered roads. Accordingly, land acquisition cost was excluded from the OCCD model by applying the objective function in Eq. 2 with the binary variable $f_4 = 0$. The other cost components were retained in the objective function to investigate the optimal design of SZC based on earthwork, lining, and water loss costs.

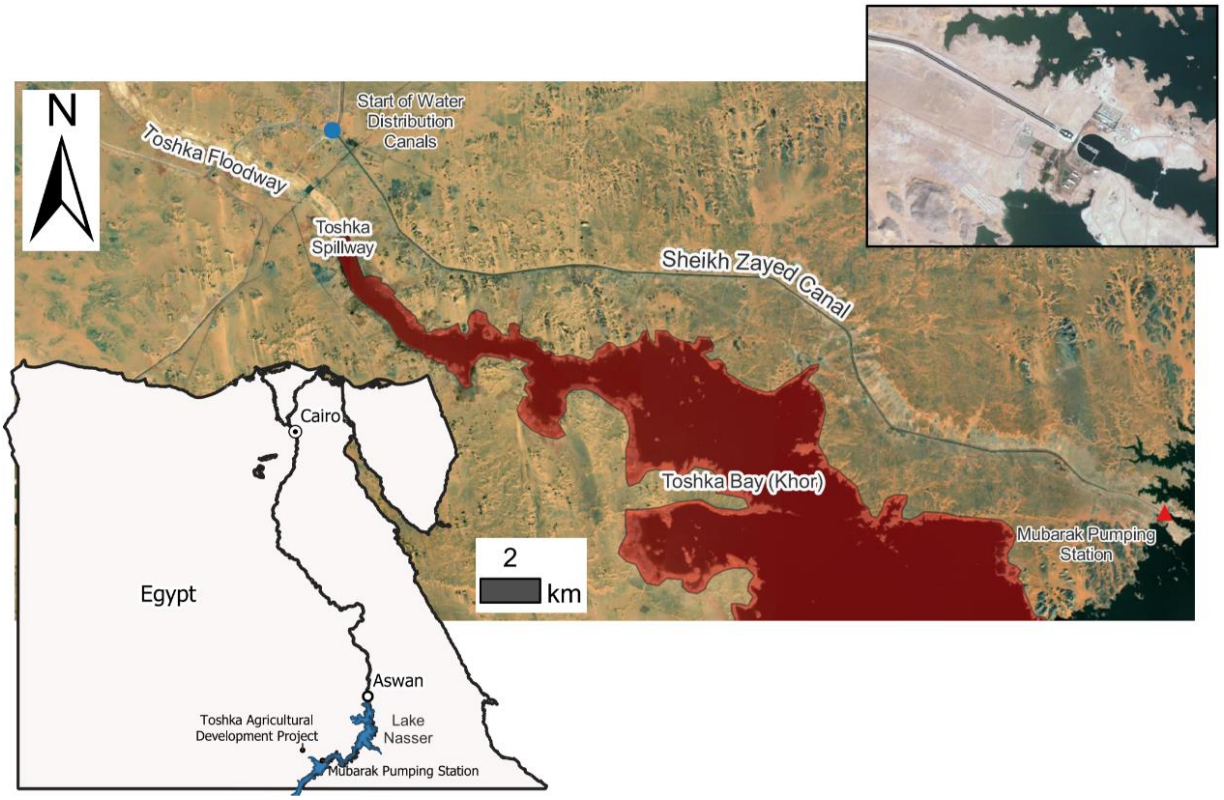

Fig. 15: The location of SZC within Toshka Agricultural Development Project in Egypt. The satellite image was captured at the end of 1998 (adapted from Google Earth). The inset in the top right shows the Mubarak pumping station and the transition channel in 2019 (adapted from ESRI Satellite Imagery).

4.2 Surrounding Topography

Topographic survey data for the SZC region were not available for this study. Instead, the ALOS digital elevation model (DEM) was used. Similar to other freely available DEMs (SRTM and ASTER), the ALOS DEM has a horizontal resolution of $30\,m \times 30\,m$ (Takaku et al., 2018). However, the ALOS DEM likely has higher vertical accuracy (Zhang et al., 2019). It was released in mid-2016, is based on the data collected after the construction of the SZC, and accordingly represents post-construction topography. To approximate the pre-construction topography along the SZC, the DEM data was adjusted by interpolation of ground elevations within a swath extending over the canal width and length (Fig. 16).

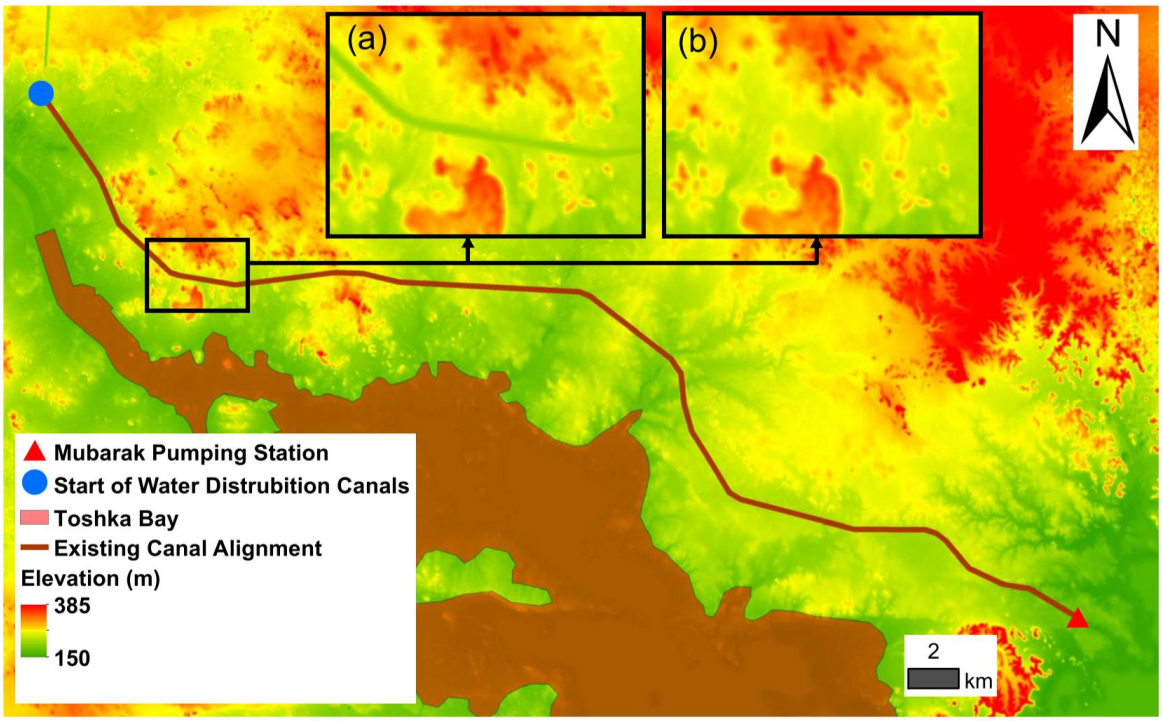

Fig. 16: Topography along and surrounding the Sheikh Zayed Canal (SZC). Insets a) and b) show a segment of SZC with a smaller scale. Inset a) represents raw ALOS DEM and inset b) represents the modified DEM after the adjustment of ground elevations along the canal alignment.

4.3 Evaporation and Seepage Losses

The SZC is in a hyper-arid region and evaporation losses from the canal are expected to be high. For the application of the OCCD model, the annual average evaporation rate was set to $E = 7.5\, mm/d$. (El Baradei and Al Sadeq, 2019). The model estimated daily evaporation flux per unit length of SZC (q_v) using,

$$q_v = E\, B \tag{14}$$

where B is the top channel width obtained from the Hydraulic Simulation module.

Similar to other lined channels, the lining in SZC cannot completely prevent seepage. Even with good maintenance and little imperfections, lining reduces seepage by only 30 to 40 % compared to seepage from unlined channels (Swamee and Chahar, 2015). To estimate seepage losses from SZC, the seepage rate with no lining was first quantified and was then adjusted by a factor of 0.35 to account for the lining. The final seepage rate per unit length of SZC (q_s) was calculated using (Swamee and Chahar, 2015),

$$q_s = 0.35kyF_s \tag{15}$$

where k is the hydraulic conductivity of the underlying soil, y is the simulated water depth, and the factor F_s is given by,

$$F_s = \left(\{[\pi(4-\pi)^{1.3}] + (2t)^{1.3}\}^{p_1} + \left(\frac{b}{y}\right)^{p_2} \right)^{p_3} \tag{16}$$

in which the exponents $p_1 = \frac{0.77+0.462t}{1.3+0.6t}$, $p_2 = \frac{1+0.6t}{1.3+0.6t}$, and $p_3 = \frac{1.3+0.6t}{1+0.6t}$. For SZC, the underlying soil is classified as clay loam (FAO et al., 2012). The hydraulic conductivity for this soil was taken as $0.22\,m/d$ (Francisco J. Tapiador, 2008).

4.4 Cost Calculations

Indicative values for the unit cost of excavation at the ground surface; cost increment per unit depth of excavation; and unit costs for fill, lining, and water losses were adapted from Irrigation & Waterways Department (2018) and Ren et al. (2018). To simplify the analysis and presentation of results, the unit costs were normalized by the excavation unit cost (e.g., the unit cost of excavation was taken as unity). The normalized unit costs for fill, lining, and water loss were set to $U_F/U_X = 1.4$, $U_L/U_X = 10\,m$, and $U_W/U_X = 0.02$, respectively. The increase in excavation cost per unit depth was set to 12 % of U_X.

The cost of water losses was calculated for 25 years which was assumed to be the duration until major rehabilitation of the canal would be performed. Conversion to present worth was not needed; the unit cost for water loss was assumed to increase by the same percentage as the interest rate.

For calculation of earthwork and lining costs, the berm level was set based on the higher freeboard obtained from the following equations (JICA and OIDA, 2014),

$$F_1 = 0.05y + 0.5h_v + h_s \tag{16}$$

$$F_2 = 0.6 + 0.036Vy^{1/3} \tag{17}$$

where y is the flow depth, V is the flow velocity, h_v is the velocity head, and h_s is the water surface oscillation range (taken as 0.1m).

4.5 Modelling Scenarios

The hydraulic analysis was first conducted for the existing canal design to calculate its cost, which was then compared to the cost of the design alternatives determined by the OCCD model. Three different scenarios were examined with the model (Tab. 4). The objective of the first scenario (SZS-1) was to identify the optimal design variables that achieve the minimum total cost. The second scenario (SZS-2) aimed to produce the optimal design variables while neglecting water losses. Finally, the third scenario (SZS-3) was used to demonstrate how the model can be applied to justify canal lining. In this scenario, the optimal design for the minimum cost of earthwork and water loss was compared with the optimal design of SZS-1.

To keep the number of design variables in the OCCD model reasonable, 14 reaches were applied in all scenarios instead of the 23 reaches making up the existing canal alignment. The Manning coefficient for scenarios SZS-1 and SZS-2 was set to 0.02 as per the existing design and was set to 0.03 in SZS-3. The geometric constraints included a restricted zone extending over Toshka Bay (Fig. 15). Maximum contraction and enlargement in bed width were limited to 20 %. Hydraulic constraints included limiting the maximum water depth to 8 m for all scenarios and limiting the maximum water velocity to $2.5\,m/s$ for SZS-1 and SZS-2 and to $1\,m/s$ in SZS-3.

Table 4: Summary of modelling scenarios for the Sheikh Zayed Canal (SZC).

Scenario	Number of reaches	Design variables	Considered costs	Manning Coeffi-cient	Maximum allowable velocity (m/s)	Maximum allowable depth (m)
SZS-1	14	Bed widths, side slopes, coordinates and elevations of intermediate junctions	$C_E + C_L + C_W$	0.02	2.5	8
SZS-2			$C_E + C_L$	0.02	2.5	
SZS-3			$C_E + C_W$	0.03	1.0	

4.6 Optimal Design Results

4.6.1 Cost of existing canal design

The hydraulic simulation of the existing SZC design showed that the flow is sub-critical with a Froude number of 0.2, a depth of $6\,m$, and a flow velocity of $1.34\,m/s$. The rate of water losses amounts to $5.9\ m^3/s$ for seepage and $0.2\ m^3/s$ for evaporation, which combined represent about 1.8% of the design discharge. The $1\,m$ freeboard can accommodate an additional discharge of $100\ m^3/s$; SZC can carry a flow of up to $444\ m^3/s$ without flooding. The existing canal profile shows that the canal passes through different high and low terrain, with maximum excavation and fill depths of $27\ m$ and $16\ m$, respectively (Fig. 19a).

The normalized present cost (NPC) of the existing canal design amounted to 1.54×10^8. The water loss cost due to seepage represented $\sim 56\%$ of the total cost whereas the evaporation losses cost represented only $\sim 2\%$ (Fig. 18). The excavation cost was more than five times the fill cost as the canal alignment passes through relatively high terrain, whereas the applied 12% increment in excavation cost accounted for $\sim 40\%$ of the overall excavation cost. Finally, the lining cost was $\sim 20\%$ less than the earthwork cost.

4.6.2 Minimum total cost scenario

The OCCD model results for SZS-1 showed that the model respected the geometric constraint and avoided crossing Toshka Bay (Fig. 17). The canal alignment produced by the OCCD model had a length of $45\ km$, shorter by 5% than the existing canal ($47.3\ km$). The alignment from the model was almost identical to the existing canal alignment at its downstream end. Along the rest of the path, the alignment from the model wiggled around and deviated from the existing alignment by up to $2.8\ km$ (Fig. 17).

The OCCD model produced a profile with reaches of variable longitudinal slope ranging from flat (i.e., horizontal) to 186 cm/km (Fig. 19b and Tab. 5a). The model generated a cross-section with a uniform side slope of 0.5 which matched the lower limit specified to the model. The canal bed width ranged between 23.5 m at the canal upstream end and 33.5 m at the downstream end with an average width of 26.8 m. Including the freeboard, the total canal depth ranged between 5.3 m and 8.7 m. The maximum excavation and fill depths were 23.5 m and 14.2 m, respectively. Compared to the maximum excavation and fill depths for the existing canal, the maximum depths for the SZS-1 design alternative were less by about 13.5%, making this alternative easier and safer to construct.

The OCCD model respected the specified hydraulic constraints. The simulated reach-average flow velocity ranged between 1.3 m/s and 2.2 m/s, lower than the maximum allowable velocity of 2.5 m/s (Tab. 5a). The simulated reach-average flow depth ranged between 7.8 m and 4.6 m, below the maximum threshold of 8 m (Fig. 19b). If the bed width in the downstream-most reach had been 30 m instead of 33.5 m to maintain a uniform width, the maximum allowable depth constraint would be violated by 0.015 m in the first 155 m of the reach, which explains why the OCCD model selected the bed width of 33.5 m. The calculated freeboard by the OCCD model ranged from 0.66 m to 0.8 m. The minimum freeboard can accommodate an additional 56 m^3/s of water, allowing the canal to carry up to 390 m^3/s without flooding (if water surface fluctuation was neglected). If a uniform freeboard of 1 m was considered, the total cost of the OCCD design would increase by 0.8%.

The NPC of SZS-1 design alternative which was produced by the OCCD model was equal to 1.17×10^8, with a significant reduction of 24% compared to the cost of the existing canal design (Fig. 18). The largest percentage of cost reduction was in the excavation cost, which decreased by approximately half. In contrast, the fill cost increased by $\sim 109\%$. A maximum cost difference of $1.78 \times 10^7$was achieved in the seepage losses cost, with a reduction percentage of $\sim 21\,\%$. Considering the capital costs only (i.e., neglecting the water losses cost), the cost of the design alternative produced by the OCCD model would be $\sim 27\%$ less than the cost of the existing canal design.

4.6.3Minimum earthwork and lining costs scenario

Similar to SZS-1, the OCCD model avoided crossing Toshka Bay in SZS-2 (Fig. 17). The produced canal alignment had a length of $46.6\ km$, longer by 3.5% than the SZS-1 alignment ($45\ km$) but shorter by 1.5% than the existing canal alignment ($47.3\ km$). The SZS-2 alignment is similar to the existing canal alignment except near the middle of the canal where it was shifted by $3\ km$ southward (Fig. 17).

Similar to SZS-1, the OCCD model selected a uniform side slope of 0.5 for scenario SZS-2. However, as the cost of water losses was not included in scenario SZS-2, the OCCD model did not tend to limit the flow width and depth to reduce seepage and evaporation losses. Compared to SZS-1, the model selected wider canal beds with larger flow depths for SZS-2 (Tab. 5b). The canal bed width for SZS-2 ranged between $24.75\ m$ and $36.25\ m$ with an average of $28.6\ m$ which is $\sim 7\ \%$ wider than for SZS-1. The reach-average flow depth for SZS-2 ranged between $5.0\ m$ and $8.0\ m$ with a mean value that is $\sim 6\%$ deeper than for SZS-1. To obtain larger flow depth and wider bed width for SZS-2, the model selected milder longitudinal slopes of no more than $34\ cm/km$ (Tab. 5b and Fig. 19c). These milder slopes allowed for lower flow velocities in the range $1.32\ m/s$ to $1.91\ m/s$.

The OCCD model respected the constraints of maximum allowable depth and velocity along the canal. Flow depth along the canal was less than 8 m and flow velocity was less than 2.5 m/s (Tab. 5b). The calculated freeboard by the OCCD model ranged between $0.66\ m$ and $0.76\ m$. The minimum freeboard can accommodate an additional $54\ m^3/s$ of water, leading to a total flow of $388\ m^3/s$. If a uniform freeboard of $1\ m$ was considered, the total cost of the OCCD design would increase by 1.9%. Considering the freeboard, the canal depth ranged between $6\ m$ and $9\ m$. The maximum excavation depth was $24.2\ m$, slightly higher than in scenario SZS-1, whereas the maximum fill depth was $13.8\ m$, slightly lower than in SZS-1.

With the exclusion of water losses cost, the NPC of the SZS-2 design alternative was 4.46×10^7 compared to 6.50×10^7 for the existing canal design. The cost reduction achieved by the SZS-2 alternative amounts to $\sim 31\%$ (Fig. 18). The largest percentage of cost reduction was in the excavation, which was $\sim 61\%$ less in SZS-2. In contrast, the fill cost increased by about $\sim 104\%$ (Fig. 18). Furthermore, the NPC of SZS-2 design alternative was $\sim 5\%$ less than the cost of SZS-1 if water losses is excluded.

Including the cost of water losses, the NPC of SZS-2 design alternative was $\sim 23\%$ less than the cost of the existing canal design, and $\sim 2\%$ more than the cost of SZS-1. The water losses cost was reduced by $\sim 17\%$ compared to the existing canal design but increased by 5% compared to SZS-1.

4.6.4Minimum earthwork and water loss cost scenario

Similar to the previous two scenarios, the OCCD model avoided crossing Toshka Bay in scenario SZS-3 (Fig. 17). The produced canal alignment had a length of $43.25\ km$, shorter by 3.8% than SZS-1 ($45\ km$). In this scenario, the OCCD model tried to shorten the length of the canal alignment despite the existence of very high terrain along the chosen alignment (Fig. 17). This indicates the dominance of the water losses cost along the canal lifetime over the earthwork cost.

Similar to the previous two scenarios, the OCCD model application to scenario SZS-3 produced a cross-section with a uniform side slope along the canal. The selected side slope of 2 corresponded to the lower limit specified in the model. This lower limit was higher than for the other scenarios (where the limit was 0.5) to maintain side slope stability given that no lining was used in SZS-3.

Compared to scenarios SZS-1 and SZS-2, the SZS-3 profile was relatively more uniform (Fig. 19d). The longitudinal slopes for the SZS-3 canal reaches ranged between 3 and $25\ cm/km$. The slopes were milder than in other scenarios to allow for lower flow velocities that would minimize erosion of the unlined canal bed in SZS-3. With a specified maximum allowable velocity of 1 m/s for SZS-3, the model produced reach-average flow velocities ranging between $0.88\ m/s$ and $0.98\ m/s$. Besides using milder longitudinal slopes, the model selected relatively wide bed widths to attain lower velocities. The canal bed width ranged between $26.5\ m$ and $36.6\ m$ with an average of $31\ m$.

Along the flow direction, the reach-average depth decreased from 8 m to 7 m; while the freeboard was almost constant at 0.66 m (Tab. 5c). The maximum excavation depth for SZS-3 reached 40.5 m, higher than in the other scenarios. Similarly, the maximum fill depth reached 19.5 m, higher than the other scenarios. The calculated freeboard by the OCCD model can accommodate an additional 57 m^3/s of water; allowing the canal to carry up to 391 m^3/s. If a uniform freeboard of 1 m was considered, the total cost of the OCCD design would increase by 0.4%.

With the cost of water losses included, the NPC of the unlined canal from scenario SZS-3 was 2.09×10^8, which is ~ 79% higher than the cost of the lined canal from scenario SZS-1 (Fig. 18). Passing through high terrain to shorten the canal length caused the excavation cost for SZS-3 to increase by ~ 248%, whereas the fill cost slightly decreased by ~ 2%. Even though the SZS-3 alignment is shorter, the cost of water losses due to seepage increased significantly by ~ 107% due to the absence of lining, whereas the evaporation losses cost increased by ~ 75% as the canal became wider. SZS-3 results support the decision made to line the canal with a concrete lining, as a lower total cost was achieved in SZS-1 compared to SZS-3.

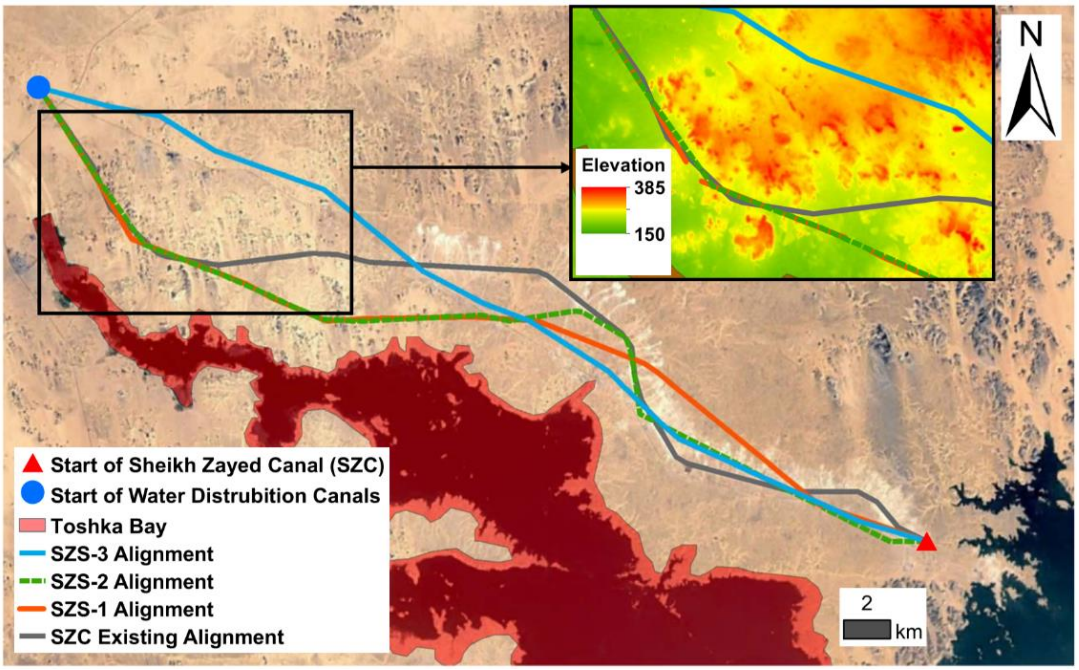

Fig. 17: Alignments selected by the OCCD model compared to the existing canal alignment. Inset shows a zoomed view of a segment of the alignments with surrounding topography in the background.

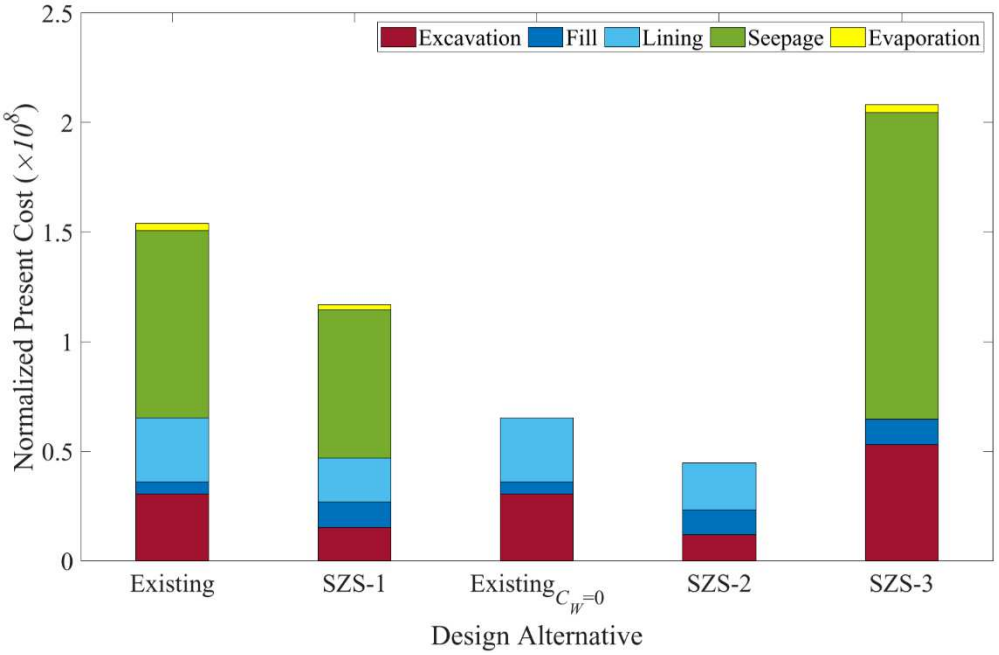

Fig. 18: NPC components for existing and OCCD model design alternatives.

Table 5: Model results for scenarios a) SZS-1. b) SZS-

Reach Number	1	2	3	4	5	6	7	8	9	10	11	12	13	14
Length (*km*)	4.87	6.67	2.31	0.59	4.92	2.70	0.20	4.42	1.73	2.60	1.22	5.21	3.60	4.02
Longitudinal slope (*cm/km*)	3	3	0	27	3	32	186	7	10	5	19	1	2	29
Side slope	0.5:1 (horizontal to vertical)													
Bed width (*m*)	23.5	24.2	25.0	28.5	27.7	30.0	32.7	28.2	26.2	25.0	25.0	25.5	28.0	33.5
Maximum canal depth with freeboard (*m*)	8.71	8.35	7.70	7.45	7.45	7.46	7.82	7.82	7.64	7.58	7.34	7.34	6.34	5.29
Reach-average flow depth (*m*)	7.82	7.32	6.81	6.70	6.47	6.47	6.94	7.02	6.89	6.72	6.60	6.14	5.11	4.56
Reach-average velocity (*m/s*)	1.56	1.64	1.73	1.57	1.67	1.56	1.33	1.50	1.63	1.75	1.79	1.91	2.15	2.05

(a)

Reach Number	1	2	3	4	5	6	7	8	9	10	11	12	13	14
Length (*km*)	1.54	12.04	2.49	0.85	2.15	0.30	2.82	1.18	5.01	1.86	4.59	3.69	3.49	4.61
Longitudinal slope (*cm/km*)	8	1	10	31	0	34	9	7	6	4	5	1	1	19
Side slope	0.5:1 (horizontal to vertical)													
Bed width (*m*)	24.75	28.25	31.25	29.75	29.25	28.50	27.00	26.50	27.25	26.50	26.00	25.75	30.25	36.25
Maximum canal depth with freeboard (*m*)	9.00	9.00	8.28	8.47	8.47	8.37	8.36	8.32	8.28	8.07	7.91	7.43	6.72	5.97
Reach-average flow depth (*m*)	7.99	7.62	7.25	7.37	7.38	7.33	7.34	7.30	7.18	7.00	6.68	6.08	5.35	4.97
Reach-average velocity (*m/s*)	1.45	1.37	1.32	1.36	1.37	1.42	1.48	1.52	1.51	1.59	1.70	1.91	1.90	1.73

(b)

Reach Number	1	2	3	4	5	6	7	8	9	10	11	12	13	14
Length (*km*)	3.03	2.10	6.36	0.89	3.32	3.97	2.20	2.83	2.64	2.86	4.94	2.80	2.11	3.21
Longitudinal slope (*cm/km*)	9	8	3	25	7	4	7	12	6	7	4	7	5	8
Side slope	2:1 (horizontal to vertical)													
Bed width (*m*)	26.50	28.25	30.50	34.50	29.25	30.00	31.00	32.00	30.50	30.00	31.75	32.50	32.75	36.50
Maximum canal depth with freeboard (*m*)	8.67	8.67	8.65	8.49	8.49	8.44	8.24	8.31	8.31	8.22	8.14	7.89	7.81	7.70
Reach-average flow depth (*m*)	8.00	7.99	7.83	7.75	7.79	7.67	7.55	7.59	7.60	7.51	7.35	7.18	7.09	7.04
Reach-average velocity (*m/s*)	0.98	0.94	0.92	0.86	0.96	0.96	0.96	0.93	0.96	0.99	0.98	0.99	0.99	0.88

(c)

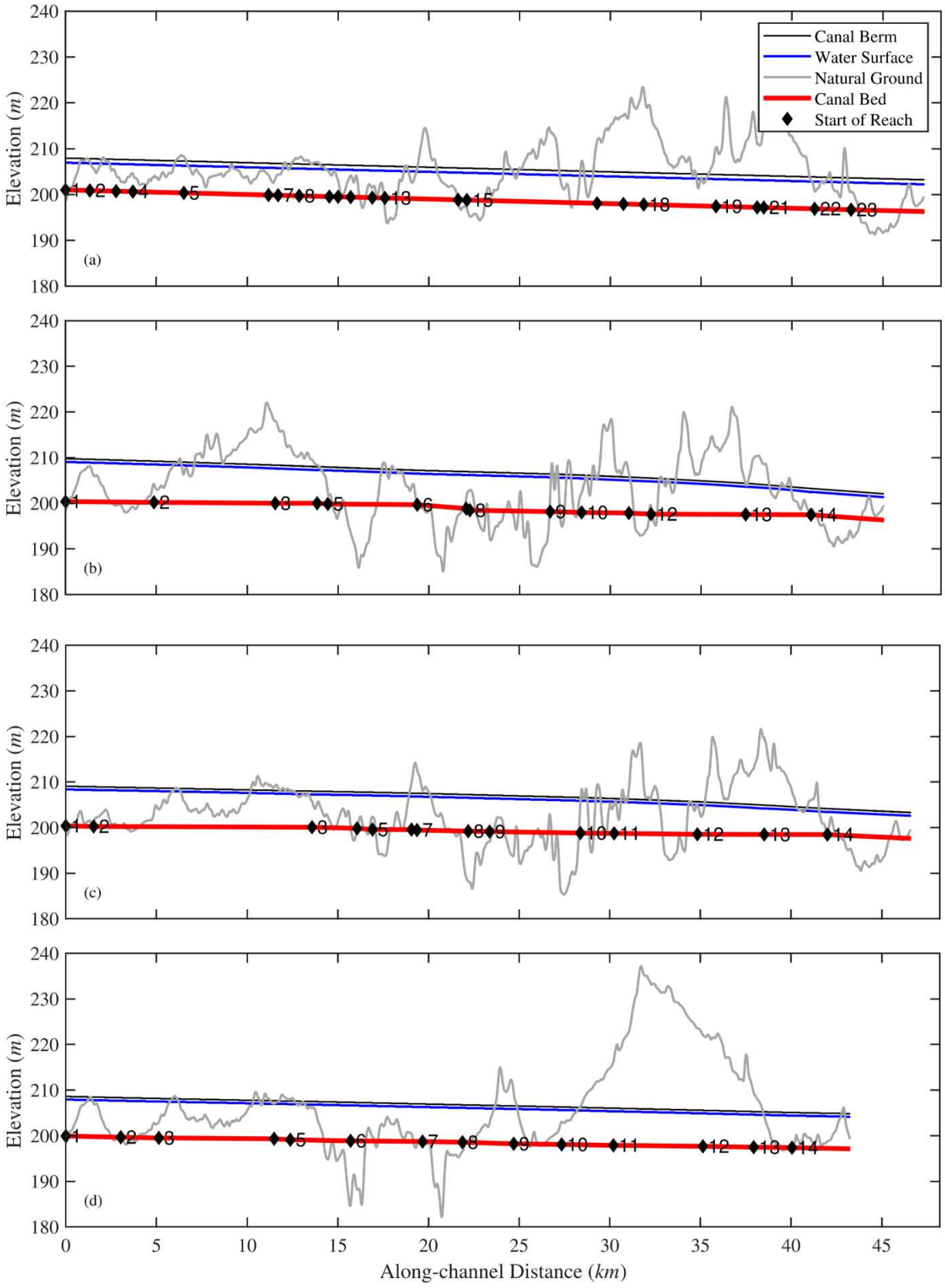

Fig. 19: a) The existing canal profile along with the profiles produced by the OCCD model for b) SZS-1, c) SZS-2, and d) SZS-3. The natural ground level was smoothed and some reach start points were removed to improve visualization.

5. Conclusions and Recommendations

In this study, an optimization model, referred to as the OCCD model, was developed to aid in the design of open channels taking into account the interdependence between the design parameters and efficiently searching through the immense number of design alternatives. Unlike traditional design methodologies, the OCCD model is capable of concurrently optimizing the channel design parameters as opposed to separating the design process into de-linked stages. The proposed OCCD model is robust, automated, and comprehensive as it accounts for various costs and considers geometric and hydraulic constraints. Furthermore, the OCCD model is compact and efficient as it includes its own Hydraulic Simulation module and requires no link to external hydraulic models.

The performance of the OCCD model was thoroughly evaluated by applying it to seven validation scenarios. The first three scenarios focused on the optimization of the channel cross-section, whereas the other four scenarios were used to confirm the ability of the OCCD model to optimize the channel profile and alignment. The results of the first three validation scenarios matched the analytical/ empirical solutions found in the literature. Similarly, the other four scenarios produced anticipated rational outcomes. These results confirmed that the model can determine the optimal channel design parameters (e.g., channel alignment, profile, and cross-section). Also, it proved that the OCCD model can handle the specified geometric and hydraulic constraints.

The model performance was further assessed by applying it to a case study; the existing Sheikh Zayed Canal in Egypt. The model was first applied to conduct a hydraulic simulation and cost analysis for the existing channel design. The model was then applied to identify the optimal design for multiple scenarios. The OCCD model produced more optimal design alternatives, with considerable cost reduction and water savings compared to the existing canal design. In one of the scenarios, the OCCD model was used to determine the feasibility of lining the SZC; model results supported the decision to line the canal and decrease seepage losses.

The methodology used in the formulation of the OCCD model (Section 2) makes the model suitable for the design of transmission open channels that convey constant discharge. Nonetheless, there are multiple possibilities for improving the OCCD model in future work. From a hydraulic point of view, it can be generalized to consider the possible variation of discharge along the channel to be suitable for designing irrigation distribution channels. This will also enable the OCCD model to account for water lost along the channel length, providing for a more optimal design. Furthermore, the model may be improved by including the spatial variation of hydraulic conductivity and climatic conditions for better estimation of seepage and evaporation losses. From an optimization point of view, the model can be improved by accounting for more detailed earthwork costs including haulage, soil import, and disposal as well as by accounting for the variation of ground level along the transverse direction of the channel alignment. In addition, the cost of inter-reach transition, as well as operation and maintenance costs, can be considered to accurately present the overall cost. Finally, other evolutionary optimization techniques may be tested to increase the efficiency and reliability of the OCCD model.

Acknowledgements The first author is thankful for Prof. Reda M. El-Damak[1] and Dr. Ashraf A. Al-ashaal[2] for providing important information and sharing some data for the Sheikh Zayed Canal.

[1] Irrigation and Hydraulics Department, Faculty of Engineering, Cairo University, Giza, Egypt

[2] Construction Research Institute, National Water Research Center, Kaliobeya, Egypt

Declarations

Consent to Publish All authors give their consent to publish.

Consent to Participate All authors give their consent to participate.

Competing Interests The authors declare no competing interests.

Availability of Data and Materials All data that support the results are available upon request.

Authors' Contributions Aly K. Salem: Conceptualized, coded, tested and analyzed the OCCD model results and wrote the manuscript. Yehya E. Imam: Assisted in conceptualizing, coding and analyzing the results, participated and reviewed the manuscript. Ashraf H. Ghanem and Abdallah S. Bazaraa: Reviewed the manuscript and gave constructive suggestions.

Funding All authors declare that no funds or other support were received for this research.

6. References

- Adarsh S, Sahana AS (2013) Minimum Cost Design of Irrigation Canals Using Probabilistic Global Search Lausanne. Arabian Journal for Science and Engineering 38(10):2631–2637, DOI 10.1007/s13369-012-0493-x
- Akan O (2006) Open Channel Hydraulics. DOI 10.1016/B978-0-7506-6857-6.X5000-0
- Aksoy B, Altan-Sakarya AB (2006) Optimal lined channel design. Canadian Journal of Civil Engineering 33:535–545, DOI 10.1139/L06-008
- Basu S, Chahar BR (2013) Optimal cutting and filling height for canal length. In: World Environmental and Water Resources Congress 2013, May, pp 2227–2236, DOI 10.1061/9780784412947.219
- Bhattacharjya RK (2005) Optimal design of open channel section considering freeboard. ISH Journal of Hydraulic Engineering 11(3):141–151, DOI 10.1080/09715010.2005.10514808
- Chahar BR (2006) Simplified design method of a transmission canal. In: Joint International Conference on Computing and Decision Making in Civil and Building Engineering, pp 436–445
- Chahar BR, Novman A, Godara R (2007) Optimal parabolic section with freeboard. Journal of Indian Water Works Association (March):43–48
- Chow VT (1959) Open Channel Hydraulics, 1st edn. McGRAW-HILL, New York, N.Y.
- Das A (2000) Optimal Channel Cross Section with Composite Roughness. Journal of Irrigation and Drainage Engi- neering 126(1):68–72, DOI 10.1061/(asce)0733-9437(2000)126:1(68)
- El Baradei SA, Al Sadeq M (2019) Optimum coverage of irrigation canals to minimize evaporation and max- imize dissolved oxygen concentration: Case study of Toshka, Egypt. International Journal of Environmental Science and Technology 16(8):4223–4230, DOI 10.1007/s13762-018-2010-6, URL https://doi.org/10.1007/ s13762-018-2010-6
- El-Ghandour HA, Elbeltagi E, Gabr ME (2020) Design of irrigation canals with minimum overall cost using particle swarm optimization - case study: El-Sheikh Gaber canal, north Sinai Peninsula, Egypt. Journal of Hydroinformatics 22(5):1258–1269, DOI 10.2166/hydro.2020.199

- FAO, IIASA, ISRIC, ISSCAS, JRC (2012) Harmonized world soil database (version 1.2). FAO, Rome, Italy and IIASA, Laxenburg, Austria, URL http://webarchive.iiasa.ac.at/ Research/LUC/External-World-soil-database/ HTML/index.html?sb=1
- Francisco J Tapiador (2008) Rural Analysis and Management: An Earth Science Approach to Rural Science. Springer- Verlag Berlin Heidelberg
- Froehlich DC (1994) Width and depth-constrained best trapezoidal section. Journal of Irrigation and Drainage En- gineering 120(4):828–835, DOI 10.1061/(ASCE)0733-9437(1994)120:4(828)
- Guo CY, Hughes WC (1984) Optimal channel cross section with freeboard. Journal of Irrigation and Drainage Engineering 110(3):304–314, DOI 10.1061/(ASCE)0733-9437(1984)110:3(304)
- Han YC, Easa SM, Gao XP (2019) General explicit solutions of most economic sections and applications for trapezoidal and parabolic channels. Journal of Hydrodynamics 31(5):1034–1042, DOI 10.1007/s42241-018-0155-x
- Haupt RL, Haupt SE (2003) Practical Genetic Algorithms. John Wiley & Sons, DOI 10.1002/0471671746 HEC (2016) HEC-RAS Reference Manual
- Irrigation & Waterways Department (2018) Unified Schedule of Rates. Tech. rep.
- Jain A, Bhattacharjya RK, Sanaga S (2004) Optimal design of composite channels using genetic algorithm. Journal of Irrigation and Drainage Engineering 130(4):286–295, DOI 10.1061/(ASCE)0733-9437(2004)130:4(286)
- JICA, OIDA (2014) Technical Guideline for Design of Headworks. Tech. rep., Japan International Cooperation Agency, Oromia Irrigation Development Authority
- King HW, Brater EF, Lindell JE, Wei CY (1949) Handbook of Hydraulics. Wiley and Sons Kramer O (2017) Genetic Algorithm Essentials. Springer
- Mathworks (2014) Optimization Toolbox User's Guide R2014b

- McCuen RH, Knight Z, Cutter AG (2006) Evaluation of the Nash–Sutcliffe Efficiency Index. Journal of Hydrologic Engineering 11(6):597–602, DOI 10.1061/(asce)1084-0699(2006)11:6(597)
- Monadi M, Mohammadi M, Taghizadeh H (2019) Optimal design of open channel sections using PSO. Iranian Journal of Optimization 11(2):207–215
- Monadjemi P (1994) General formulation of best hydraulic channel section. Journal of Irrigation and Drainage Engi- neering 120(1):27–35
- Niazkar M (2020) Assessment of artificial intelligence models for calculating optimum properties of lined channels. Journal of Hydroinformatics 22(5):1410–1423, DOI 10.2166/hydro.2020.050
- Niazkar M, Afzali SH (2015) Optimum Design of Lined Channel Sections. Water Resources Management 29(6):1921– 1932, DOI 10.1007/s11269-015-0919-9
- Ren Y, Wei S, Cheng K, Fu Q (2018) Valuation and pricing of agricultural irrigation water based on macro and micro scales. Water (Switzerland) 10(8):1–13, DOI 10.3390/w10081044
- Simpson AR, Dandy GC, Murphy LJ (1994) Genetic algorithms compared to other techniques for pipe optimization. Journal of Water Resources Planning and Management 120(4):423–443, DOI 10.1061/(asce)0733-9496(1994)120: 4(423)
- Swamee PK (1994) Normal-depth equations for irrigation canals. Journal of Irrigation and Drainage Engineering 120(5):942–946, DOI 10.1061/(ASCE)0733-9437(1994)120:5(942)
- Swamee PK, Chahar BR (2013) Optimal alignment of a canal route. Proceedings of the Institution of Civil Engineers - Water Management 166(8):422–431, DOI 10.1680/wama.11.00097, URL https://www.icevirtuallibrary.com/ doi/10.1680/wama.11.00097
- Swamee PK, Chahar BR (2015) Design of Canals. Springer Transactions in Civil and Environmental Engineering, Springer Transactions in Civil and Environmental Engineering, URL https://link.springer.com/content/pdf/ 10.1007/978-81-322-2322-1.pdf

- Swamee PK, Mishra GC, Chahar BR (2000a) Comprehensive design of minimum cost irrigation canal sections. Journal of Irrigation and Drainage Engineering 126(5):322–327
- Swamee PK, Mishra GC, Chahar BR (2000b) Design of minimum seepage loss canal sections. Journal of Irrigation and Drainage Engineering 126:28–32, DOI 10.1061/(ASCE)0733-9437(2000)126:1(28)
- Swamee PK, Mishra GC, Chahar BR (2000c) Minimum cost design of lined canal sections. Water Resources Man- agement 14:1–12, DOI https://doi.org/10.1023/A:1008198602337
- Tabari MM, Mari M (2016) The Integrated Approach of Simulation and Optimization in Determining the Opti- mum Dimensions of Canal for Seepage Control. Water Resources Management 30(3):1271–1292, DOI 10.1007/ s11269-016-1225-x
- Tabari MM, Tavakoli S, Mari M (2014) Optimal Design of Concrete Canal Section for Minimizing Costs of Water Loss, Lining and Earthworks. Water Resources Management 28(10):3019–3034, DOI 10.1007/s11269-014-0652-9 Takaku J, Tadono T, Tsutsui K, Ichikawa M (2018) Quality improvements of 'AW3D' global DSM derived from ALOS
- PRISM. In: International Geoscience and Remote Sensing Symposium (IGARSS), IEEE, DOI 10.1109/IGARSS. 2018.8518360
- Trout TJ (1982) Channel design to minimize lining material costs. Journal of the Irrigation and Drainage Division 108:242–294
- Wahby WS (2002) The Toshka project of Egypt: a multidisciplinary engineering education case study. In: ASEE Annual Conference Proceedings, pp 4671–4682
- Yeniay Ö (2005) Penalty function methods for constrained optimization with genetic algorithms. Mathematical and Computational Applications 10(1):45–56, DOI 10.3390/mca10010045
- Yeo MF, Agyei EO (1998) Optimizing engineering problems using genetic algorithms. Engineering Computations (Swansea, Wales) 15(2-3):268–280, DOI 10.1108/02644409810202684

- Zhang K, Gann D, Ross M, Robertson Q, Sarmiento J, Santana S, Rhome J, Fritz C (2019) Accuracy assess- ment of ASTER, SRTM, ALOS, and TDX DEMs for hispaniola and implications for mapping vulnerability to coastal flooding. Remote Sensing of Environment 225(November 2018):290–306, DOI 10.1016/j.rse.2019.02.028